A Microfabricated Bioimpedance Sensor with Enhanced Sensitivity for Early Breast Cancer Detection

Vaishnavi Srinivasaraghavan

Thesis submitted to the faculty of the
Virginia Polytechnic Institute and State University
in partial fulfillment of the requirements for the degree of

Master of Science
In
Electrical Engineering

Masoud Agah, Committee Chair
Jeannine S. Strobl
Elankumaran Subbiah

1st December, 2011
Blacksburg, VA

Keywords: Breast Cancer, Bioimpedance, Microelectrodes, SAHA, Biosensor

A Microfabricated Bioimpedance Sensor with Enhanced Sensitivity for Early Breast Cancer Detection

Vaishnavi Srinivasaraghavan

ABSTRACT

Bioimpedance is the term given to the complex impedance value that is characteristic of the resistance that biological cells offer to the flow of electric current. The impedance measured is a function of the frequency of the AC voltage applied and a lot of information can be gained by making measurements over a large frequency range. At higher frequency ranges (>10 kHz), as the interior of the cells is being probed, different biological cells display variations in their bioimpedance properties.

The objective of this study is to analyze the differences in the bioimpedance of highly metastatic MDA-MB-231 and normal MCF 10A breast epithelial cells and use this information to detect a very small number of breast cancer cells present in a background of normal breast cells and other cells that are typically present in a human biopsy sample.

To accomplish this, a bioimpedance sensor with flat gold microelectrodes on a silicon substrate was designed and fabricated. Suberoylanilide hydroxamic acid (SAHA), an FDA-approved anti-cancer agent was used to improve the sensitivity of the bioimpedance sensor towards cancer cells by selectively modifying their cytoarchitecture. The geometry of the microelectrodes was optimized to improve the sensitivity of the sensor to the cytoskeletal changes in cancer cells induced by the chemical stimulus (SAHA). Fibroblast cells are relevant to the study as they are present in breast tissues and were included in the cell model to test the ability of the sensor to handle complex cell cultures with multiple cell types. The above improvements resulted in a bioimpedance sensor with enhanced sensitivity capable of detecting a single MDA-MB-231 cancer cell present on an electrode in a background of up to 100 normal MCF 10A breast cells and HS68 fibroblast cells.

Sriramajayam

Acknowledgements

I am extremely grateful to Dr. Masoud Agah the director of VT MEMS and my advisor for giving me the opportunity to work on this project. He has been a very interesting person to know and interact with and has been a source of inspiration and support throughout my life at Virginia Tech. I am also highly indebted to Dr. Jeannine Strobl for always having faith in the data I generate and making me a believer in my work. I would like to thank Dr. Elankumaran Subbiah for agreeing to be on my committee and offering me advice and help during the course of the project. I look forward to collaborating with him in the future.

The students of VT MEMS Lab, Bassam Alfeeli, Phillip Zellner, Yahya Hosseini, Hamza Shakeel, Muhhamad Akbar and Hesam Babahosseini, have been an entertaining bunch to know and befriend. Mehdi Nikkhah and Shree Narayanan deserve a special mention for sharing their experience and throwing light on the intricacies of doing research.

My friends, Mrudula Karve, Kalyani Tipnis, Aditi Chaudhry, Saparya Krishnamoorthy and Swati Sudhaakar, and all the people I met at Virginia Tech. who I will always remember for making life in Blacksburg a fun affair.

I would like to acknowledge my father, P. Srinivasaraghavan, who has always been and will continue to be my role model and a source of motivation throughout my life and my mother, Usha Jagannathan, for her unconditional love and support for everything I do. My sister, Varshini Srinivasaraghavan, also warrants a mention for pushing me to be a person that she would look up to.

Finally, I would like to thank God for all the blessings he has showered on me and for where I am today.

Table of Contents

1. Introduction 1
2. Background 4
    2.1. Electric Cell-Substrate Impedance Sensing (ECIS) 4
    2.2. Electrical Circuit Model 7
3. The Role of SAHA 9
    3.1. Chemistry. 9
    3.2. Effect on Cell Cytoskeleton and Area 10
    3.3. SAHA and Bioimpedance 14
4. First Generation Bioimpedance Sensor 15
    4.1. Design and Fabrication 15
    4.2. Experiments 18
        4.2.1. Measurement Setup 18
        4.2.2. Cell Culture 19
        4.2.3. Bioimpedance Measurements 19
    4.3. Results 20
    4.4. Discussion 23
5. Second Generation Bioimpedance Sensor 24
    5.1. Design and Fabrication 24
    5.2. Experiments 26
    5.3. Results 26
    5.4. Discussion 30
6. Tri-cell Culture Model 32
    6.1. Rationale 32
    6.2. Experiments 32
    6.3. Results 33
    6.4. Discussion 37
7. Conclusion 38
8. References 39

List of Figures

Chapter 2

Figure 2.1: The two most commonly used electrode structures to perform bioimpedance Spectroscopy 5

Figure 2.2: Electric circuit used to model the bioimpedance of cells adherent to Electrodes 7

Chapter 3

Figure 3.1: The chemical structure of suberoylanilide hydroamic acid (SAHA) 9

Figure 3.2: The comparison of the effect of 2.75μM SAHA on the mean cell area of MDA-MB-231 and MCF 10A cells 11

Figure 3.3: Fluorescence images of the three cell types in monoculture on flat gold without and with 500 nM SAHA 12

Figure 3.4: The comparison of the effect of 500nM SAHA on the mean cell area of MDA-MB-231 and MCF 10A cells 13

Chapter 4

Figure 4.1: Optical image of the first generation bioimpedance sensor is shown along with the electrode configuration 15

Figure 4.2: The process flow used to fabricate the bioimpedance sensor 17

Figure 4.3: The comparison of the changes seen in the peak bioimpedance value of MDA-MB-231 and MCF 10A cells in five randomly selected electrodes due to 2.75μM SAHA 21

Figure 4.4: Scatter plot of the peak impedance rise due to SAHA (2.75 μM) versus the number of cancer cells on each electrode from co-culture experiments on the first generation bioimpedance device 22

Figure 4.5: Unconstrained spreading of cancer cell on a wide electrode (right) versus constrained spreading of cancer cells on narrow electrode (left) under the effect of SAHA 23

Chapter 5

Figure 5.1: Conceptual illustration of the bioimpedance sensor 24

Figure 5.2: Optical image showing the bioimpedance sensor along with an enlarged

schematic of the electrode configuration 25
Figure 5.3: The bioimpedance changes due to SAHA (500 nM) on the cancer and normal cell types over three randomly selected electrodes from three experiments with four microelectrodes in each device 27
Figure 5.4(A): Fluorescence images from a co-culture experiments (MCF10A cells – Red; MDA-MB-231 cells – Green) 29
Figure 5.4(B): A typical plot of normalized impedance over the frequency range seen on all the electrodes from an experiment; each color represents a separate electrode 29
Figure 5.4(C): The characteristic real-time changes in peak bioimpedance magnitude on a single electrode when SAHA is introduced 29

Chapter 6

Figure 6.1: The changes in the peak bioimpedance seen due to 500 nM SAHA over three randomly selected electrodes for each of the three cell types 34
Figure 6.2: Fluorescence image highlighting the three cell types on an electrode in a tri-culture experiment 35
Figure 6.3: SAHA induced responses in the presence (electrodes 1-4) and absence (electrodes 5-8) of cancer cells on the peak bioimpedance in eight randomly selected electrodes 36

1. Introduction

Breast cancer, one of the most commonly diagnosed types of cancer, is the cause of death of approximately 40,000 people each year and has one of the highest rates of recurrence in the United States [1]. Currently, a combination of screening techniques such as noninvasive examination, mammography coupled with ultrasound or magnetic resonance imaging (MRI) and biopsies are used for clinical diagnosis. It is known that early detection of breast cancer can significantly improve the patient's prognosis and treatment [2]. An important current research focus is the identification of new biomarkers and technologies that provide reliable indicators of breast cancer prognosis and response to treatment very early in the disease process. To address this need, we have explored the use of bioimpedance spectroscopy in detecting and differentiating human breast cancer cells from normal human cells.

Electrical Cell-substrate Impedance Sensing (ECIS) is a technique that was introduced by Giaever and Keese to monitor biological cells based on the properties of cell attachment to the substrate [3]. It is a non-invasive technique where the cells are plated on flat gold electrodes present in a cell culture chamber and the AC impedance of cell-covered electrodes is measured over a range of frequencies. This is a highly sensitive technique as any changes in the cell attachment and shape alter the current flow through and around the cell. ECIS has been used to monitor various properties of cells including attachment and spreading [3-5], motility [6, 7] and growth and proliferation [8]. The technique also lends itself to studies of the response of cells to drug treatment in real time [9, 10]. The properties of single cells within a population of cells can be analyzed to better understand cellular activity and heterogeneity at single cell levels [11-15]. Comparison studies between conventional and impedance-based methods aimed at characterizing cell proliferation confirm that bioimpedance measurements can indeed be used as an indicator of these properties when properly calibrated [16]. Electrodes used for impedance measurements can be easily integrated into microfabricated devices [13]. Advances in microelectromechanical systems (MEMS) such as batch fabrication, low

cost, integration with electronics and microfluidic components make it a promising approach to design ECIS-based silicon biosensor chips to gauge changes in cellular physiology.

Over the last decade, there has been increasing support for the idea that the ECIS technique is a valuable tool to analyze cancer cells. Liu et al. cultured human oesophagal cancer cells (KYSE 30) on microelectrodes coated with fibronectin to study their response to the anti-cancer drug cisplatin [17]. Cellular activity and drug induced apoptosis of oral squamous cell carcinoma (OSCC) using ECIS were studied by Arias et al. [18]. Also, differences between the cancerous OSCC cell line and the non-cancerous oesophagal epithelial cell line (Het-1A) were investigated using the impedance response with a commercially available Real Time-Cell Electronic System (RT-CES) [19]. Cho et al. studied the bioimpedance responses of highly and poorly metastatic Head and Neck (HNC) cells and reported statistical differences in the phase angle of their corresponding impedances[20]. Single cell analysis of differences between non-cancerous MCF10A and breast cancer cell lines MDA-7 (early stage), MDA-MB-231 and MDA-MB-435 (metastasized) was done by Han et al [21]. In their paper, the magnitude and phase of measured impedance over the frequency range 100 Hz to 3 MHz and also the differences in membrane capacitance and resistance at 100 kHz obtained through modeling were reported. Thus, it is well established that bioimpedance measurements reveal important information about the condition of malignant cell(s), and under specific circumstances, have been shown to distinguish between cancerous and normal cells in individual cultures. To our knowledge, there are no published reports on ECIS to detect the presence of cancer cells when cultured simultaneously with other types of cells.

A silicon-based ECIS chip for cancer cell detection is reported here that exploits the principle that differential cellular physiology among cells will result in distinguishable bioimpedance signatures. We used highly metastatic MDA-MB-231 breast cancer cells, non-tumorigenic breast epithelial MCF10A cells and human fibroblast HS68 cells to represent cell types commonly present in human breast biopsy samples. The following sections describe the design and fabrication of the sensor and

how single-cancer cell detection was achieved using an anti-cancer agent (SAHA) to chemically focus the response on MDA-MB-231 cells. The long-term objective of this approach is production of an inexpensive, easy to use bioimpedance sensor that enables rapid detection and prognostic evaluation of early stage human breast cancer.

2. Background

Bioimpedance is a property of biological cells that refers to their ability to offer resistance to the flow of electric current. The bioimpedance spectroscopy of a sheet of cells adherent to flat electrodes is called Electric Cell-Substrate Impedance Sensing (ECIS) after the pioneers of the technology, Giaever and Keese [22], coined the term. In this method, the attachment of the cells to the substrate plays a major role in the bioimpedance characteristics that are observed. The gap between the cell and the substrate has a direct correlation with the attachment of the cells. A well-attached cell has a smaller cell-substrate gap as opposed to a loosely bound cell, which has a much larger cell-substrate gap. It has been shown that well-attached cells offer a higher resistance to the flow of current and thus have a larger bioimpedance and vice versa. The following sections discuss the origin of ECIS and its current use as a technology and the electric circuit model of ECIS.

2.1 Electric Cell-Substrate Impedance Sensing (ECIS)

The term ECIS is a trademark of the company Applied BioPhysics Inc. It refers to a non-invasive method used to monitor biological cells in culture by measuring the dielectric properties of a confluent layer of cells on two-dimensional electrodes deposited at the bottom of a culture dish or substrate. Giaever and Keese first measured the bioimpedance of human embryonic lung fibroblast (WI 38) cells in 1984 [23]. Subsequently, they studied the micromotion of WI 38 cells, the effect of Cytocholasin B (a chemical that prevents cell division and inhibits cell movement) on the fluctuations in bioimpedance measured and the transepithelial impedance of Madin-Darby canine kidney (MDCK) cell monolayers among other things. Their technique used a combination of a large counter electrode and a smaller sensing electrode to make bioimpedance measurements. In an alternate technique, researchers used Inter-Digitated Electrodes (IDES) in which, the electrode and the counter electrode have the same comb-like

structure and are interchangeable [24]. Both techniques have been equally adopted by researchers and have shown to be sensitive to changes in morphology of cells adherent on the electrodes. However, it is unclear whether one is advantageous over the the other?. Figure 1 shows an example of the two commonly used electrode structures used to make bioimpedance measurements.

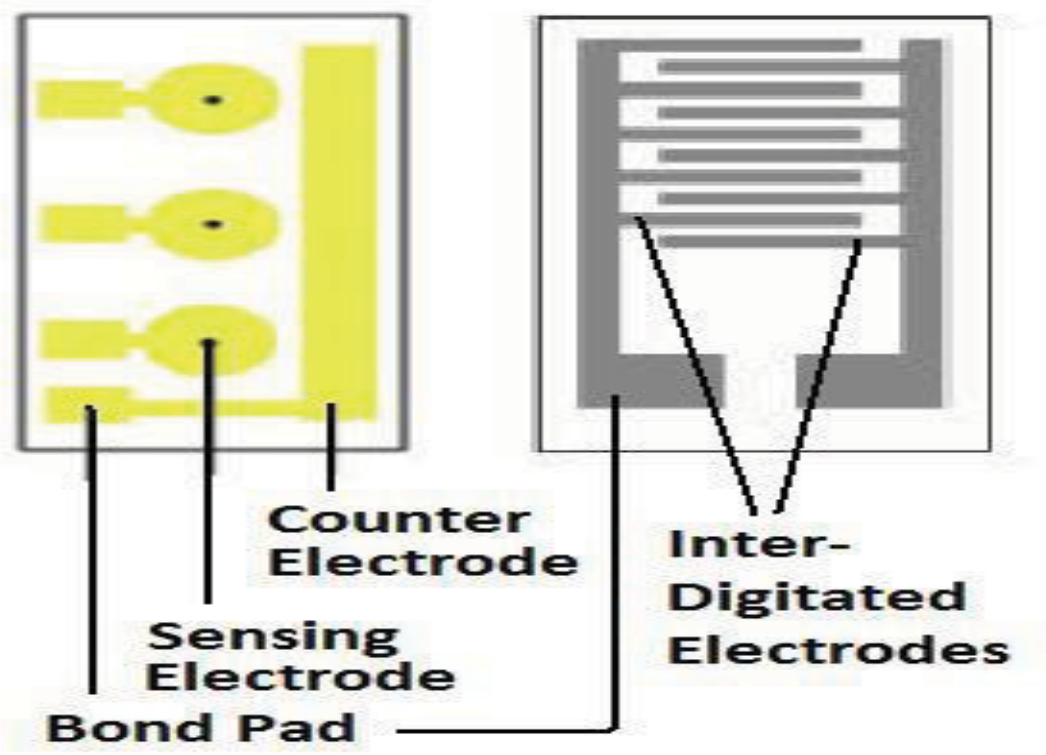

Figure 2.1. The two most commonly used electrode structures to perform bioimpedance spectroscopy.

The large counter electrode with the small sensing electrode structure was first used by Giaever and Keese [23] and adopted by their company Applied Biophysics Inc. in their products ECIS Zθ, ECIS Z and ECIS 8Z, which allow measurement of the bioimpedance of cells adherent to 250 μm diameter electrodes over multiple preset frequencies or at a single user defined frequency in an 8, 16 or 96 well culture platform. The inter-digitated electrode structure is also commercially marketed by ACEA Biosciences Inc. for use with their Xcelligence system. In this system, the bioimpedance of cells adherent to their unique inter-digitated electrodes deposited in standard cell

culture plates with 16, 96 and 384 wells can be measured at a specific present frequency and a dimensionless parameter called the cell index (CI), which is the relative change in the cell bioimpedance, is extracted from the data and used to analyze various changes in the cell morphology, adhesion, proliferation etc. Both instruments have been widely used and have been credited with publications. Some of them are [25-33] for the instrument from Applied Biophysics Inc. and [34-41] for the Xcelligence system from ACEA Biosciences Inc. and more can also be found on their respective websites.

The products above as well as the electrode structures used, require confluent cell coverage on the electrodes. Changes in a single cell have been hard to measure even though the promise of sensitivity using this technique has been repeatedly reinforced. In our bioimpedance sensor, we sought to achieve this single cell sensitivity through design of a new electrode structure that is inspired by the above designs as well as the use of a chemical stimulus, which was specific to only one type of cell.

2.2 Electric Circuit Model

Biological cells have a poorly conducting cell membrane, which houses a highly conductive cell interior. The bioimpedance of biological cells measured using ECIS can be modeled using an electric circuit like the one shown in Figure 2.2.

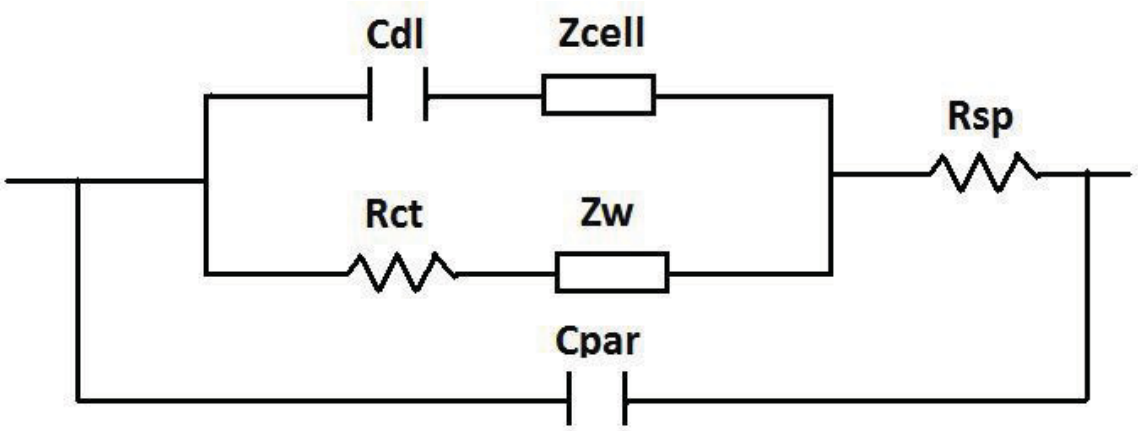

Figure 2.2. Electric circuit used to model the bioimpedance of cells adherent to electrodes.

The cell culture medium is a highly ionic solution with a high electrical conductivity, which is typically ~ 0.015 $\Omega^{-1}cm^{-1}$. In the absence of cells, the parameter Zcell in the above model will be eliminated and the equivalent circuit will resemble the Randles circuit used to model the impedance of electrodes in ionic liquids. This consists of an interfacial capacitance due to the Helmholtz double layer at the metal-electrolyte interface and the diffuse layer, which is depicted by Cdl in the above model. The charge transfer resistance (Rct) and Warburg impedance (Zw) together model the impedance of a faradic reaction. Rsp is the spreading resistance, which represents the resistance encountered when current flows from a metal electrode to the bulk of the electrolyte. Cpar represents the parasitic capacitance in the entire setup and measurement system. Commonly the entire circuit in the absence of cells is denoted by a constant phase element with n ~ 0.67.

When cells are present on the electrode, the bioimpedance measured is largely affected by different parameters in the circuit model in different frequency ranges. The cells on the electrode are not completely attached to the surface of the electrode. They make contact through focal adhesion regions, which could be only about 15-20% of the entire cell area [42]. At lower frequencies, the current due to the applied potential is unable to flow through the cell due to high impedance offered by the cell membrane, which results in the current flowing around the cell. Thus, the impedance of the double layer largely affects the impedance in this frequency range. For frequencies greater than 10 kHz, the presence of the cells affects the bioimpedance measured and a peak in the plot of the normalized impedance over frequency characterizes this, which is seen later in Figure 5.4(B). At very high frequencies, the spreading resistance limits the flow of current and thus the bioimpedance value is almost a constant. Also, parasitic capacitance starts playing a role at very high frequencies and thus the measurements are limited by the quality of the measurement setup.

3. The Role of SAHA

SAHA, also commercially known as Vorinostat and marketed under the name of Zolinza, belongs to a class of compounds called histone deacetylase inhibitors. The Food and Drug Administration (FDA) approved it on the 6th of October, 2006 for the treatment of Cutaneous T Cell Lymphoma (CTCL) [43-45]. It has also been used to treat other types of lymphoma such as the Sézary syndrome [46]. A clinical trial also showed activity of Vorinostat against recurrent glioblastoma multiforme, which resulted in an increase in the median survival rate [47]. Further clinical trials of SAHA on brain and other tumors are in progress.

3.1 Chemistry

The chemical name for SAHA according to the chemical nomenclature developed by the International Association of Pure and Applied Chemistry (IUPAC) is *N*-hydroxy-*N*'-phenyl-octanediamide. The chemical structure of the compound is shown below.

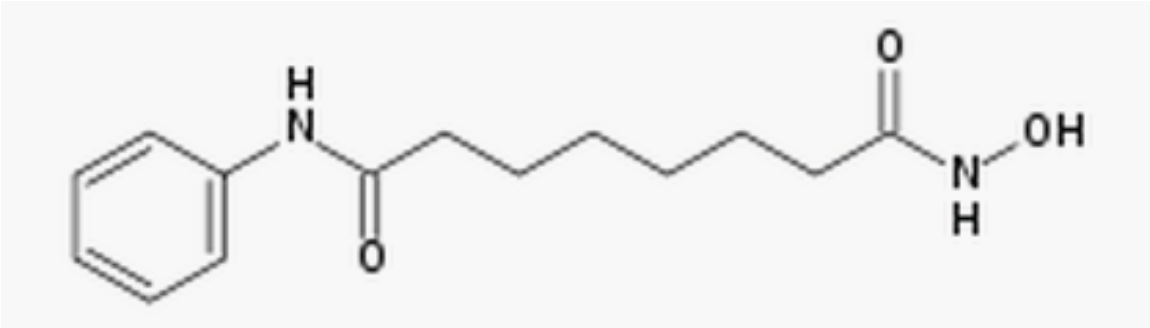

Figure 3.1. The chemical structure of suberoylanilide hydroamic acid (SAHA).

SAHA belongs to a group of compounds called histone deacetylase inhibitors that were originally discovered on the basis of their ability to interfere with the function of histone deacetylases. Histone deacetylases are enzymes that are responsible for the removal of acetyl ($O=C-CH_3$) groups from histone proteins around which, the DNA is

wrapped. Hence they can cause a variety of epigenetic changes in the cell and affect gene expression [48].

3.2 The Effect on Cell Cytoskeleton and Area

An interesting action of SAHA action is the reorganization in the cell cytoskeleton. It has been reported that SAHA causes changes in many proteins associated with the structural components of the cell cytoskeleton but has not been fully studied as yet. However, it has been shown to be associated with an increased actin expression [49]. This causes the cells to stretch and anchor to the substrate through actin rich cell extensions, which results in an overall increase in the mean cell area, which has been shown here.

The effect of SAHA (2.75μM), on the mean cell area of the cancerous MDA-MB-231 and non-tumorigenic MCF 10A cells (which we use as a model for normal breast cells) was studied. Transfected cancer (MDA-MB-231) and normal (MCF 10A) cells with green fluorescence protein (GFP) and cherry red protein, respectively were obtained from our collaborator Dr. Eva Schmelz to enable fluorescence imaging of the cells. The cells were harvested from a confluent cell cultures growing in T-75 flasks and plated on a flat silicon substrate. The cells were allowed to attach to the substrate for 20 hours after which, 2.75μM SAHA was added to the cell culture medium. After 15 hours, fluorescent images were taken using a Carl-Zeiss upright fluorescence microscope with a color (Axio Cam MRc) camera using a 20X objective.

The area of the cells was measured using the public domain NIH image processing software called ImageJ. The scale was set by drawing a straight line across the length of the scale bar on the image and setting the value of its length in micrometers. The periphery of a cell in the image was then traced and the software measured the area enclosed in units specified by the set scale. This was repeated for many cells in at least 50 different images and the average of the cell area was calculated for each cell type. The

average cell area of the control condition MCF 10A cells was 1071 ± 254 μm^2 and after SAHA (2.75μM) treatment, the average cell area was measured to be 1237 ± 205 μm^2. Similarly, the average cell area of the control condition MDA-MB-231 cells was 1066 ± 589 μm^2 and the SAHA (2.75μM) treated cancer cell area averaged at 1920 ± 795 μm^2. This was an 85% increase in the mean cell area of the cancer cells compared to the 25% seen in the normal cells. The statistical significance of these results has been previously discussed in [49]. A bar graph showing the SAHA-induced change in the mean cell area is shown in Figure 3.2.

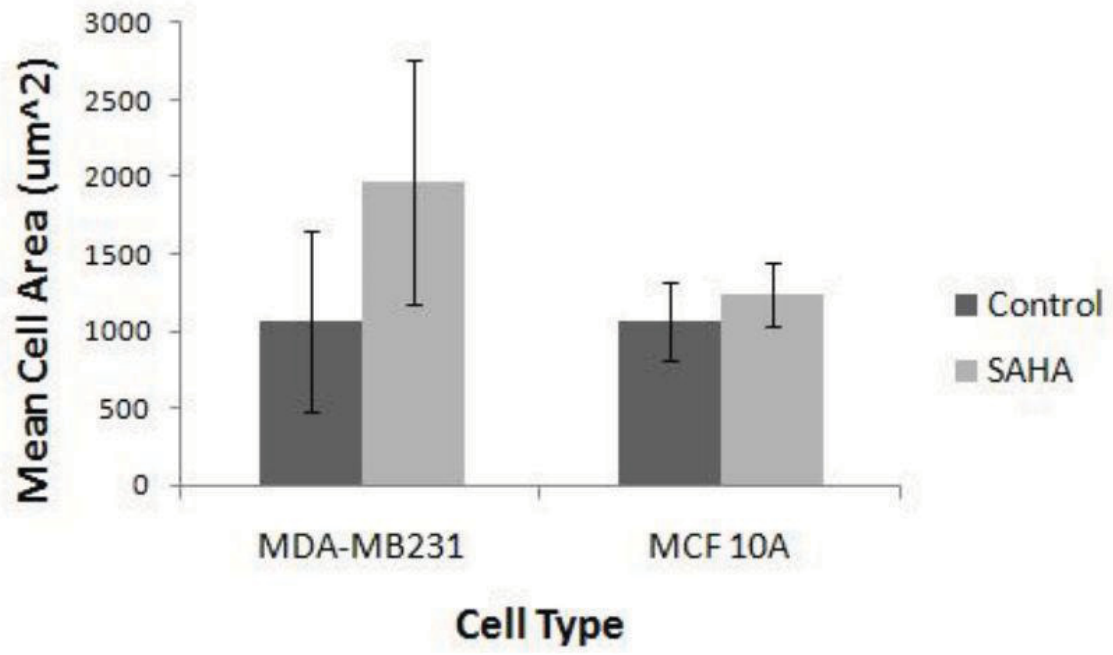

Figure 3.2. The comparison of the effect of 2.75μM SAHA on the mean cell area of MDA-MB-231 and MCF 10A cells.

As is seen clearly from the bar graph in Figure 3.2, although 2.75μM SAHA causes a significantly larger increase in the area of the MDA-MB-231 cells as compared to the MCF 10A cells, it does cause a modest 25% increase in the area of the MCF 10A cells. With the aim of reducing and possibly eliminating the SAHA-induced change in area of the MCF 10A cells, the concentration of SAHA was reduced to 500nM. The effect of 500nM SAHA on cancerous MDA-MB-231, normal MCF 10A, and HS 68

fibroblast cells was then studied. The rationale for introducing HS 68 cells will be clarified in Chapter 6. Transfected MDA-MB-231 (GFP) and MCF 10A (Cherry Red) and the HS 68 cells stained with the orange Cell Tracker dye were used in the cell area measurements. The cells were harvested from confluent cell cultures and plated on flat gold. They were allowed to attach for 20 hours after which, SAHA (500nM) was added. After another 15 hours of SAHA action, fluorescence images were taken. The fluorescence images are shown in Figure 3.3.

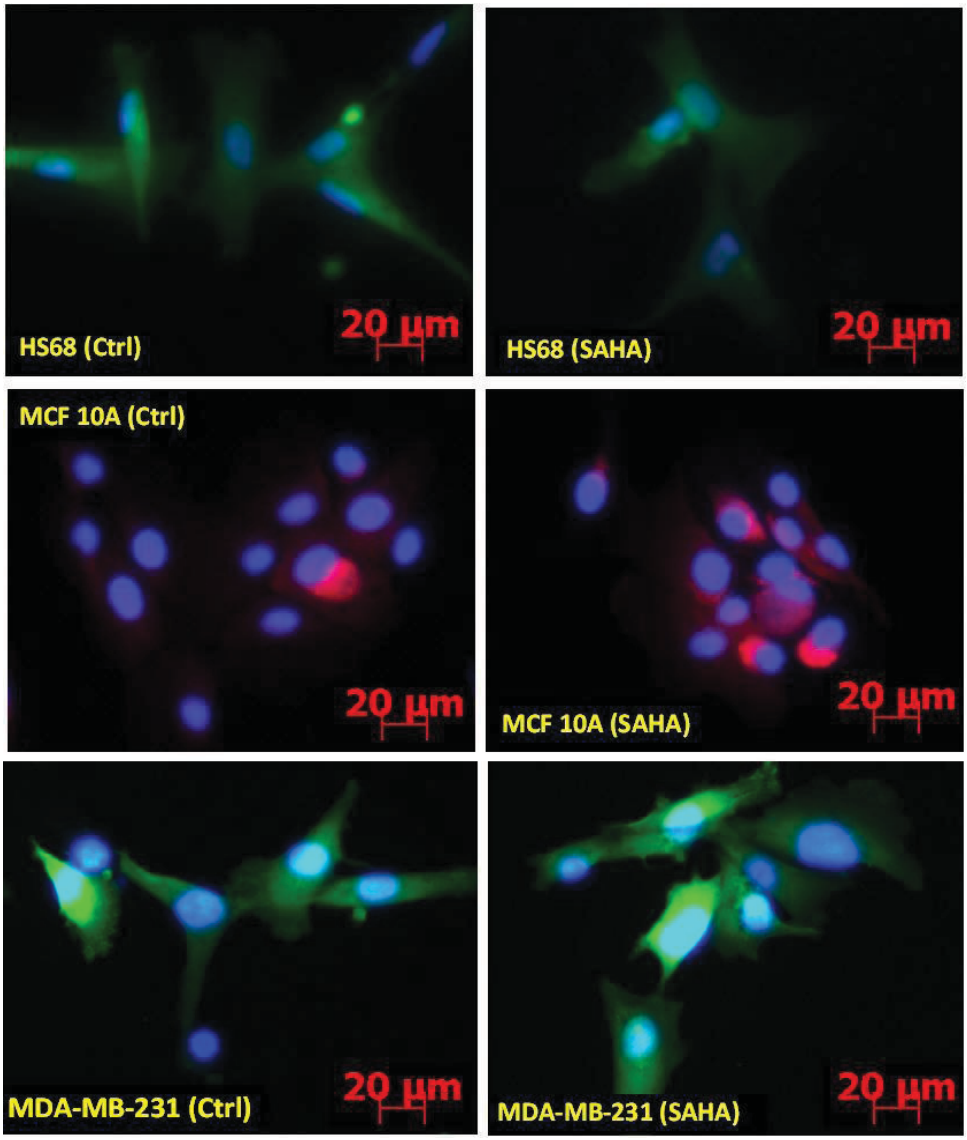

Figure 3.3. Fluorescence images of the three cell types in monoculture on flat gold without and with 500 nM SAHA.

The area of the cells was obtained from ImageJ using the method as described earlier. For the control condition MCF 10A cells, the mean cell area was found to be 750 ± 659 μm^2 and after 15 hours of SAHA action the mean cell area was measured to be 751 ± 384.16 μm^2. Similarly, the mean cell area of the control condition HS 68 cells was 1259 ± 192 μm^2 and the SAHA treated HS 68 cells had a mean cell area of 1260 ± 295 μm^2. On the other hand, the MDA-MB-231 cancer cells showed a significant increase in the mean cell area even when treated with the reduced 500nM concentration of SAHA. The control condition MDA-MB-231 cells had a mean cell area of 806 ± 134 μm^2 and when treated with 500nM SAHA the mean cell area increased to 1425 ± 127 μm^2 (Figure 3.4).

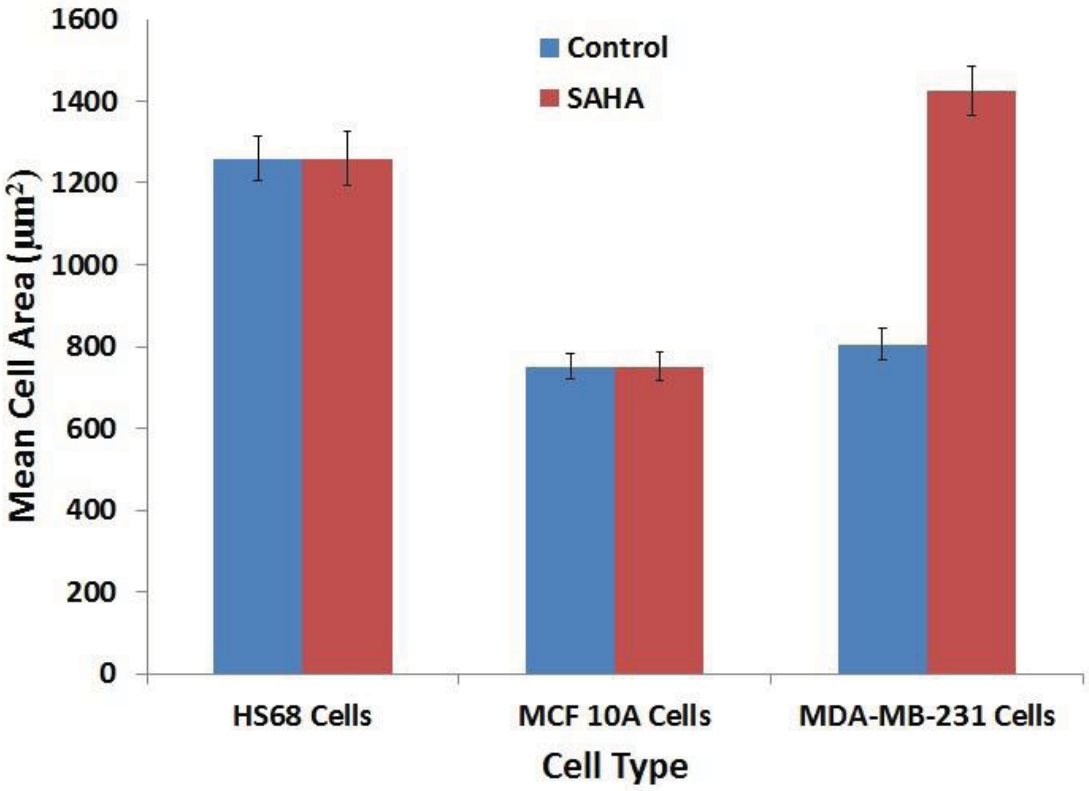

Figure 3.4. The comparison of the effect of 500nM SAHA on the mean cell area of HS68, MCF 10A and MDA-MB-231 cells.

It is clearly seen that the mean cell areas of the normal breast epithelial MCF 10A cells (two sample $t(136) = 0.013$, $P = 0.99$) and the HS 68 (two sample $t(99) = 0.013$, $P = 0.99$) fibroblasts are not significantly changed by the 500 nM SAHA treatment. The

percentage changes in the mean cell area of the MCF 10A and HS 68 cells was less that 0.01% for both cell types while the increase in the mean cell area of 500 nM SAHA treated MDA-MB-231 cells was significantly higher (two sample $t(64) = 8.454$, $P < 0.0001$) at 77%. This increase was comparable to the 85% increase seen in the mean cell area of MDA-MB-231 cells treated with 2.75 μM SAHA. Thus, it can be concluded that the reduction in the concentration of SAHA in the cell culture medium from 2.75 μM to 500 nM almost completely eliminates the SAHA-induced changes in the cell area of the MCF 10A and HS 68 cells while not compromising the SAHA action associated changes in the mean cell area of the MDA-MB-231 cells, which is still significantly high at ~77% for 500 nM SAHA. The area of the MCF10A cells was averaged over all the cells present in a colony. We attribute the large variation in the measured size of MCF10A cells to their growth in colonies; nevertheless, the data suggest that 500nM SAHA had no effect on MCF10A size.

3.3 SAHA and Bioimpedance

SAHA, as discussed above, causes a significant increase in the mean cell area of the MDA-MB-231 cells as compared to the MCF 10A and HS 68 cells. This probably results in the SAHA-treated MDA-MB-231 cells to be tightly bound or well attached to the substrate thus resulting in a larger bioimpedance value recorded as compared to the MCF 10A and HS 68 cells. Thus, bioimpedance can be used to distinguish between the cancerous MDA-MB-231 cells and the normal MCF 10A breast epithelial and HS 68 fibroblast cells. Also, when MDA-MB-231 cells are present in a co-culture or tri-culture with the above cell types, we can use SAHA as a chemical stimulus to elicit a signal from only the MDA-MB-231 cells as it is highly selective. Thus the bioimpedance sensor can be sensitized to the presence of breast cancer cells using the anti-cancer agent SAHA and can be used to detect the presence of cancer cells when they are present in a background with other cells on the sensor.

4. First Generation Bioimpedance Sensor

The first generation bioimpedance sensor was designed to study the effect of electrode shape and size on the bioimpedance of breast cells (cancer and normal). This chapter describes the design of the bioimpedance sensor, its fabrication, the experiments conducted, results obtained and discussion of the results.

4.1 Design and Fabrication

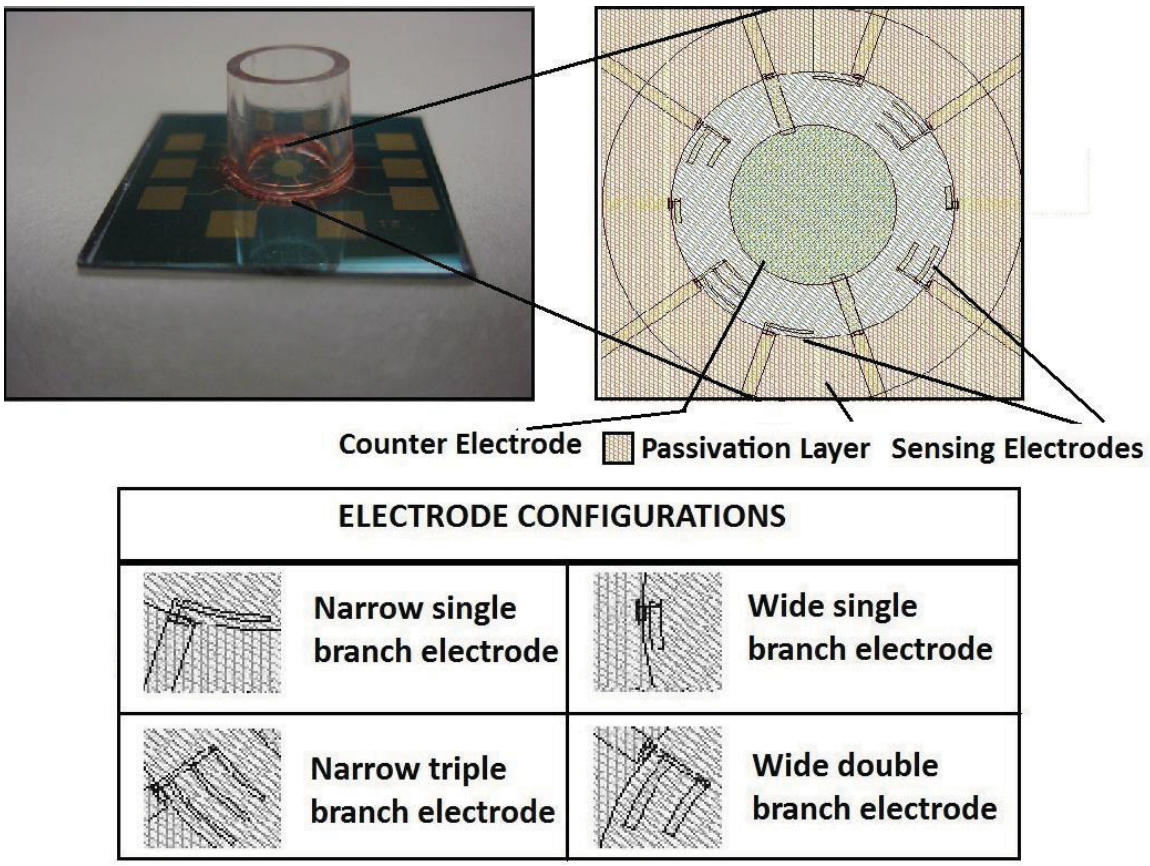

Figure 4.1. Optical image of the first generation bioimpedance sensor is shown along with the electrode configuration.

The bioimpedance sensor consists of eight sensing gold electrodes radially positioned around a large counter electrode on a flat passivated silicon substrate. The electrode configuration is shown in Figure 4.1. There are four types of electrodes in the design namely the narrow single branch electrode, narrow triple branch electrode, wide single branch electrode and wide double branch electrode. This electrode configuration helps us study the effect of a narrow branched structure, wide branched structure and number of branches on the sensitivity of the bioimpedance sensor. The narrow electrodes were 40 μm wide and the wide electrodes were 80 μm wide. The counter electrode had a diameter of 2400 μm. The sensing area in the bioimpedance sensor is defined by a second passivation layer of photoresist, which opens a circular window with a diameter of 4030 μm. The second passivation layer is a circular band of width 3950 μm surrounding the sensing area under which, a radial arms of length 5000 μm run to connect the electrodes to bond pads, which are square shaped of size 3000 μm (Figure 4.1).

The sensor was fabricated according to the process flow shown in Figure 4.2. A sterile silicon wafer was used as the starting material. An oxide layer approximately 5000 Å thick was grown on the silicon wafer using thermal oxidation in an oxidation chamber (Figure 4.2a). The wafer was then coated with photoresist (Shipley 1827) about 2 μm thick using a binder Hexamethyldisilazane (HMDS) by spin coating (Figure 4.2b). Next, the photoresist was patterned using the first mask containing the electrode design, (Figure 4.2c). A 250 Å/1500 Å Cr/Au layer was then deposited on the wafer using deposition-beam evaporation technique (Figure 4.2d). The wafer was left in acetone overnight and then placed in a sonic bath to ensure complete lift off (Figure 4.2e).

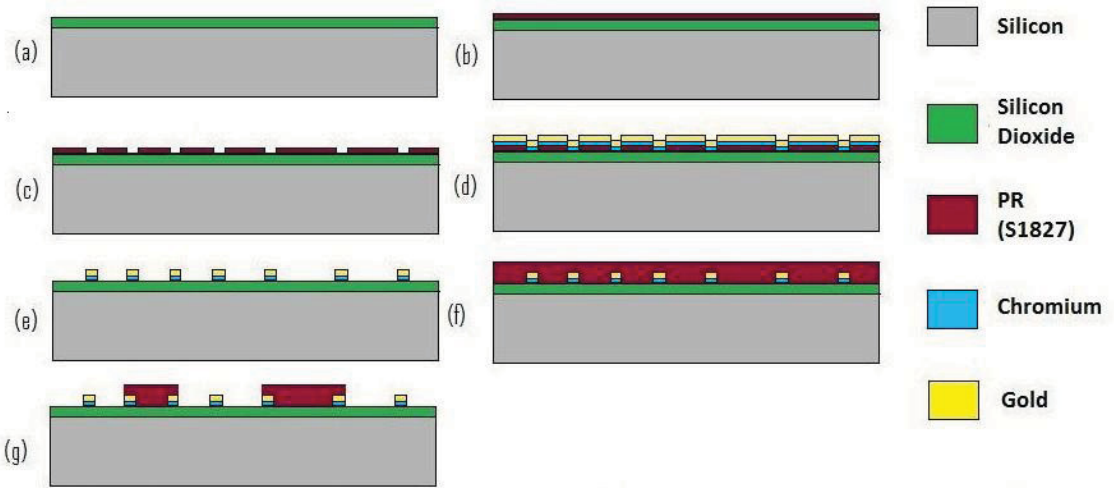

Figure 4.2. The process flow used to fabricate the bioimpedance sensor.

A 2 μm-thick photoresist layer was once again spun coated on the wafer (Figure 4.2f) and patterned using the second mask to form the passivation layer (Figure 4.2g). The wafer containing multiple devices was then diced to yield individual bioimpedance sensor chips. These chips were packaged with a cloning cylinder (Fischer Scientific: 14-512-79) around the sensing area to contain the culture medium with the cells for experimentation. They were affixed with photoresist to prevent leakage of the cell culture medium.

4.2 Experiments

The bioimpedance sensor fabricated in section 4.1 was used to conduct experiments and study the bioimpedance characteristics of the cancerous and normal breast cells. The experiments were designed to study the electrical properties of the MDA-MB-231 and MCF 10A cells separately through monoculture experiments and study the SAHA effect on the bioimpedance measurements. Based on the results obtained, co-culture experiments with both types of cells were conducted to test the ability of the sensor to detect cancer cells in a background of normal cells. The following sections describe the measurement setup and methods used to culture the cells and make bioimpedance measurements.

4.2.1 Measurement Setup

The measurement setup used has been previously published in [50]. The bioimpedance sensor unit was placed inside an incubator (NAPCO 8000WJ) maintained at 37 ˚C in a 5% CO_2 / 95% air atmosphere to support cell culture. Individual diced and packaged bioimpedance sensor chips were electrically connected to the impedance measurement setup by soldering the connecting wires to metal pads on the sensor placed inside a culture dish. The electrodes were isolated from the rest of the setup using an opto-coupler. A multiplexer and relay setup switched between the four electrodes every 30 minutes, and an impedance analyzer (HP 4192A, Agilent) was used to sweep through a frequency range and collect measurements. The complete system was controlled by a LabVIEW VI program on a computer workstation, which also stored the impedance values for analyses.

4.2.2 Cell Culture

The MDA-MB-231 and MCF10A cell lines used in this study were obtained from American Type Culture Collections (ATCC). The MDA-MB-231 and MCF10A cells were stably transfected with green fluorescence protein and cherry red protein, respectively (gift from Dr. Eva Schemelz), to enable us to capture fluorescent images of the electrodes and sensing area after every experiment. Standard cell culture methods were used for cell propagation. The cells were grown in T-75 cm^2 culture flasks in the incubator maintained at 37 ˚C and 5% CO_2. MDA-MB-231 cell culture medium consisted of DMEM with 10% fetal bovine serum (FBS) while the culture medium for the MCF10A cells consisted of DMEM with 5% horse serum, cholera toxin (CT) (100 ng/ml), hydrocortisone (0.5 mg/ml), penicillin-streptomycin (100U each/ml), insulin (10 µg/ml) and epidermal growth factor (EGF) (20 ng/ml). The cells were counted and suspended in 200µl of respective culture media for the monoculture experiments before being introduced into the cloning cylinder of the bioimpedance sensor. MCF10A cell culture medium was used for the multi-cell culture experiments We set the cell density at 8000 cells/200 µl for the monoculture experiments and 6000 cells/ 200µl for the multi-cell culture experiments. The viability of the cells was above 95% under our assay conditions.

4.2.3 Bioimpedance Measurement

The bioimpedance was monitored continuously over a period of 35 hours with measurements made every 30 min. The bioimpedance was monitored over a frequency range of 1 kHz-1 MHz to enable identification of the peak value of the normalized bioimpedance. After allowing sufficient time for the cells to attach to the sensor (20 hours), SAHA (2.75 µM) was introduced in the culture medium in the cloning cylinder. The bioimpedance was continuously monitored for a period of 15 hours after the addition of SAHA. At the end of the experiment, images of sensing area were taken using a

fluorescent microscope (Carl-Zeiss AxioLab A1 Microscope). Normalized impedance values in our experiments were calculated using the formula

$$Z_{norm} = \frac{Z_t - Z_{med}}{Z_{med}} \quad (1)$$

Z_{norm} is the normalized impedance value, Z_t is the impedance at time *t*, and Z_{med} is the impedance when only the culture medium is present. The images were cross examined and correlated with the bioimpedance values.

4.3 Results

As discussed in Chapter 3, SAHA selectively targets the cytoskeleton of cancer cells, which results in a cancer specific rise in the mean cell area and cell length. This change in cytoskeletal organization is reflected in the bioimpedance values recorded. An increase in the value of the normalized bioimpedance at the peak frequency was observed and the changes in the absolute value of the bioimpedance at the peak frequency, which we will call peak bioimpedance, due to 2.75 μM SAHA were compared for the highly metastatic MDA-MB-231 and normal MCF 10A cells. A bar graph comparing the increase in the peak bioimpedance value due to SAHA action in five randomly selected electrodes for each cell type is shown in Figure 4.3.

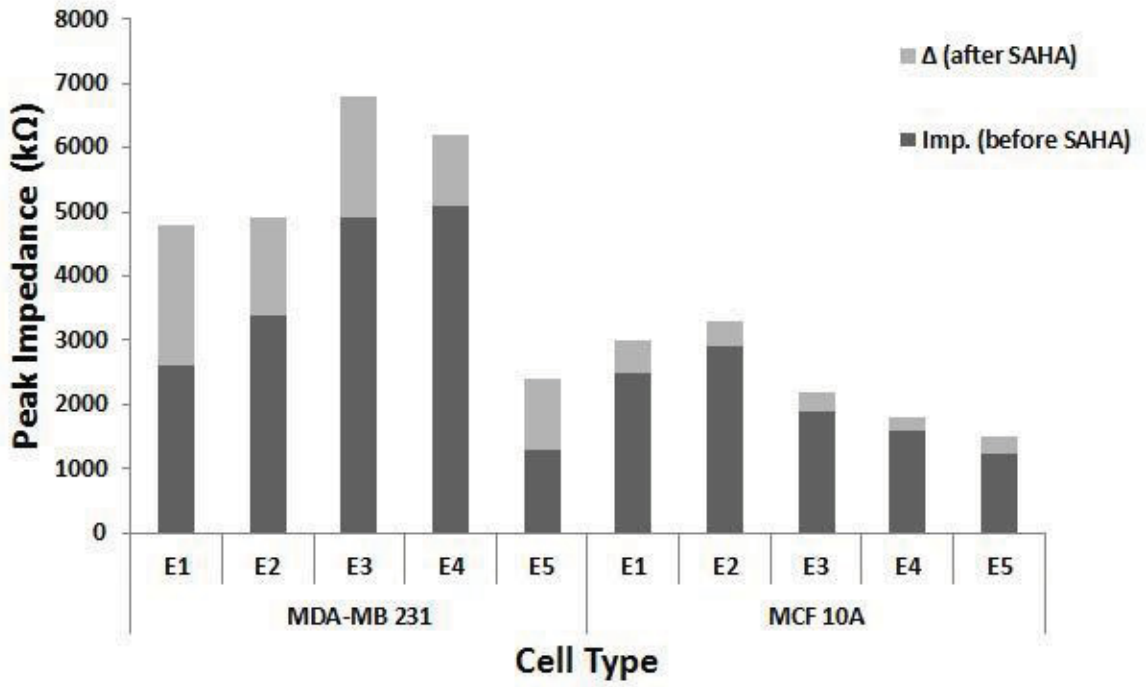

Figure 4.3. The comparison of the changes seen in the peak bioimpedance value of MDA-MB-231 and MCF 10A cells in five randomly selected electrodes due to 2.75 μM SAHA.

The average percentage increase of the peak bioimpedance value in response to 2.75μM SAHA in MDA-MB-231 cells was 175%, which was significantly higher than the corresponding value of 28% observed in MCF 10A cells. The average increase peak bioimpedance value due to SAHA for the MDA-MB-231 cells was 1560 kΩ compared to the significantly smaller 330 kΩ for the MCF 10A cells. This is clearly reflected in the plot seen in Figure 4.3.

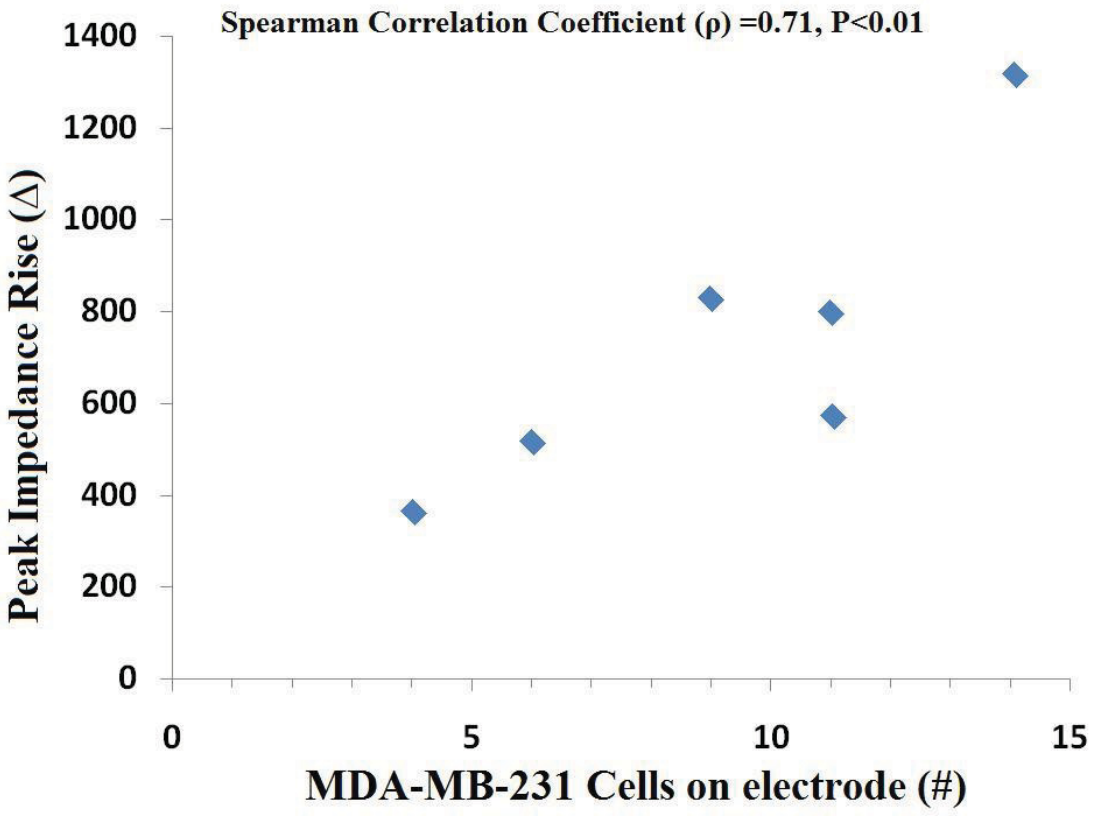

Figure 4.4. Scatter plot of the peak impedance rise due to SAHA (2.75 μM) versus the number of cancer cells on each electrode from co-culture experiments on device shown in the first generation bioimpedance device.

The results obtained from the monoculture experiments showed promise for the detection of MDA-MB-231 cells in co-culture with MCF 10A cells using SAHA as a chemical stimulus to cause a cancer cell specific rise in the bioimpedance. Mixed co-culture experiments were conducted and the rise in peak bioimpedance obtained from all four electrode configurations due to the addition of SAHA in the culture medium was correlated with the number of cancer cells on the electrode. It is important to note that only electrodes that had 10 or more total number of cells recorded reproducible signals. These electrodes showed a significant rise in impedance and detected cancer cells in co-culture experiments where the cancer to normal cell ratio was as low as 0.09. A spearman analysis (Figure 4.4) showed the impedance rise and the number of cancer cells on the electrode were significantly ($P<0.01$) correlated (coefficient (**ρ)** of 0.71). However, a

minimum of four cancer cells and at least 10 total cells had to be present on an electrode in order to be detected by the bioimpedance sensor.

4.4 Discussion

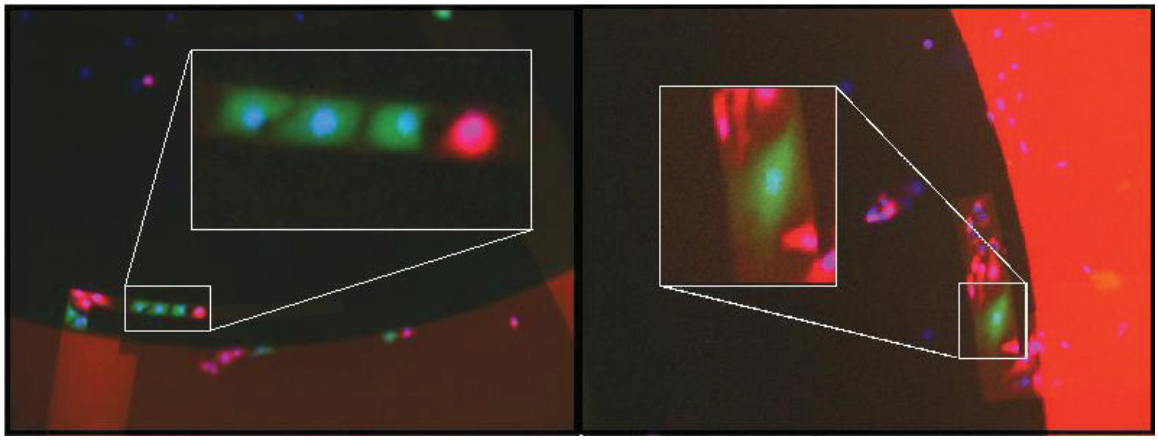

Figure 4.5. Unconstrained spreading of cancer cell on a wide electrode (right) versus constrained spreading of cancer cells on narrow electrode (left) under the effect of SAHA is shown.

The width of the electrodes can have direct influence on the SAHA-induced response of cancer cells. We designed and implemented a single narrow (40 μm) and a single wide (80 μm) branch electrode, and compared the bioimpedance response of cells to SAHA. The average increase in the peak bioimpedance values for MDA-MB-231 monoculture of cells in response to SAHA was 1075 kΩ and 725 kΩ for the narrow and the wide design, respectively. We observed the same trend in the co-culture experiments using these two electrode configurations. The enhanced sensitivity obtained might be attributable to the constrained spreading of cancer cells along the electrode boundary as compared to the uninhibited spreading seen in wide branches, which can be seen in Figure 4.5 through images obtained from co-culture experiments. Note that the breast cancer cells are green and the normal breast cells are red. This inspired the second generation of the bioimpedance sensor, which is discussed in the next chapter.

5. Second Generation Bioimpedance Sensor

In order to exploit the higher sensitivity of the narrow branch electrodes and improve the detection limits of the bioimpedance sensor, the second generation of the sensor was designed. The following sections describe the design, fabrication, experiments conducted, observed results and discussion of the significance of the results.

5.1 Design and Experiments

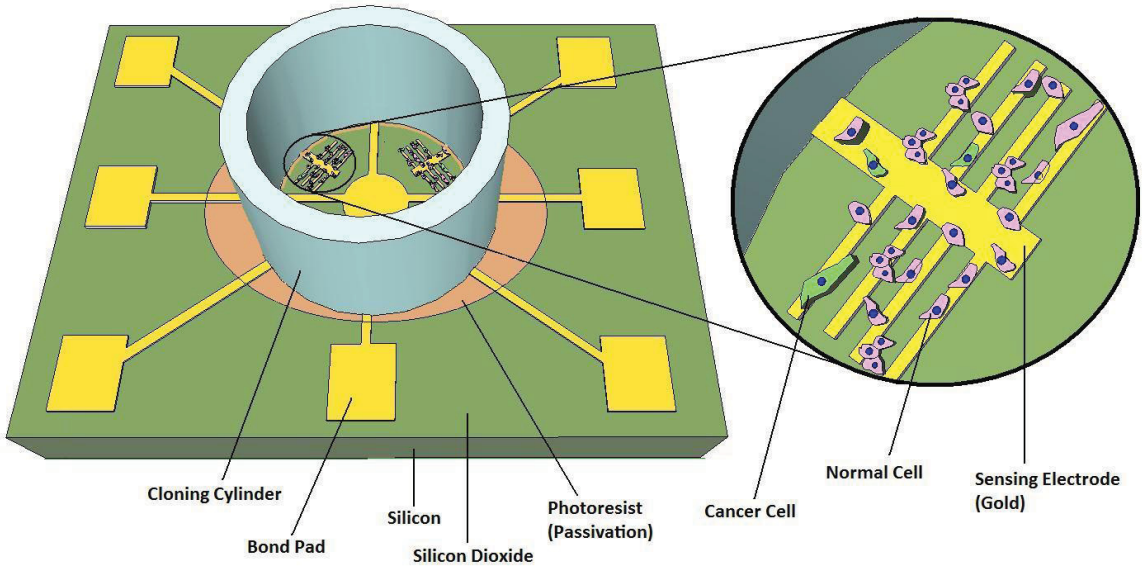

Figure 5.1. Conceptual illustration of the bioimpedance sensor.

Figure 5.1 shows the schematic of the bioimpedance sensor. A large counter electrode (2.4 mm diameter) in the center was used to minimize the potential drop over it and to make the sensing electrode more receptive to the bioimpedance changes. Narrow branches of electrodes, 40 μm-wide and 650 μm-long separated by 130 μm, were designed to enhance bioimpedance translation of the changes in cell attachment and spreading. The electrode branches were designed so that their width was comparable to

the size of the cells used in our analyses. Also multiple branches result in improved electrode coverage in the sensing area of the bioimpedance sensor, which enhances the chance of detection of sparsely present cancer cells. The bioimpedance sensor chips were packaged with a cloning cylinder with a capacity of 300 µl. This was done by affixing the cylinder around the sensing area of the bioimpedance sensor, using photoresist to prevent leakage, and held the cell culture medium and the cells during experiments.

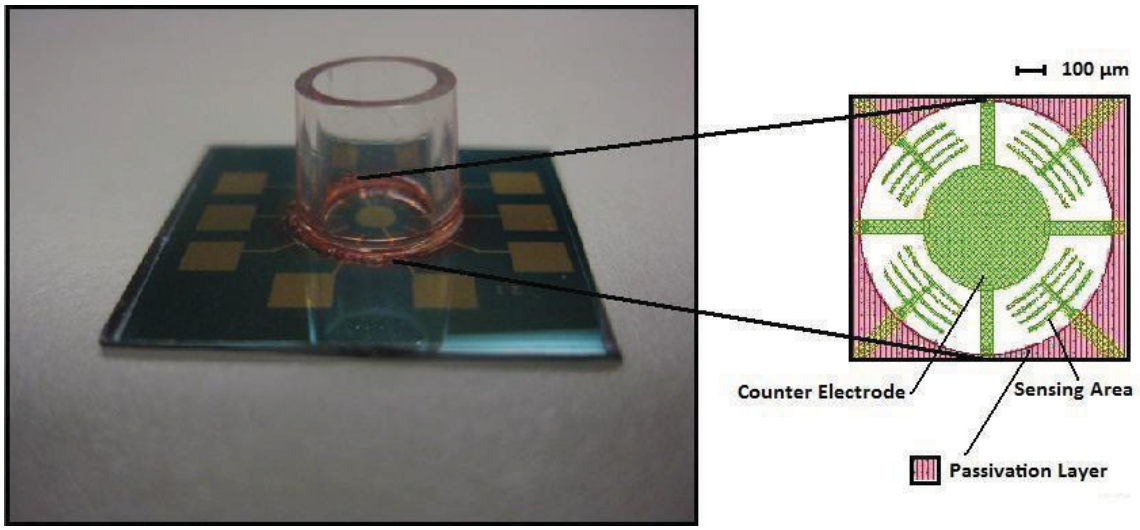

Figure 5.2. Optical image showing the bioimpedance sensor along with an enlarged schematic of the the electrode configuration.

Figure 5.2 shows that there is four identical electrodes radially arranged around the counter electrode and all of them were connected to bond pads through radial arms similar to the design of the first generation bioimpedance sensor. There was a passivation layer to define the sensing area, which was also similar to the previous design. The fabrication of the sensor followed the same process flow shown in Figure 4.2 and discussed in Section 4.1.

4.2 Experiments

The experimental procedure is similar to the description provided in Chapter 4. Please refer to Section 4.2 for further details. However, two important changes were made. First, the concentration of the anti-cancer agent SAHA introduced in the culture medium was reduced from 2.75 μM to 500 nM. This was done to reduce the change in the bioimpedance signal due to the SAHA action on the MCF 10A cells and improve the detection limits in co-culture of MCF 10 A and MDA-MB-231 cells. Also, the upper limit of the frequency range of the bioimpedance measurements made was increased from1 MHz to 12 MHz.

4.3 Results

The bioimpedance response of monocultures of malignant breast and non-malignant breast epithelial cells, before and after the introduction of SAHA (500 nM), into the culture medium, was analyzed using the bioimpedance sensor (shown in Figure 10). The SAHA induced bioimpedance change (Δ) corresponding to the peak frequency at which, the peak in normalized impedance occurs was compared over three randomly selected electrodes from different experiments and is shown in Figure 5.3.

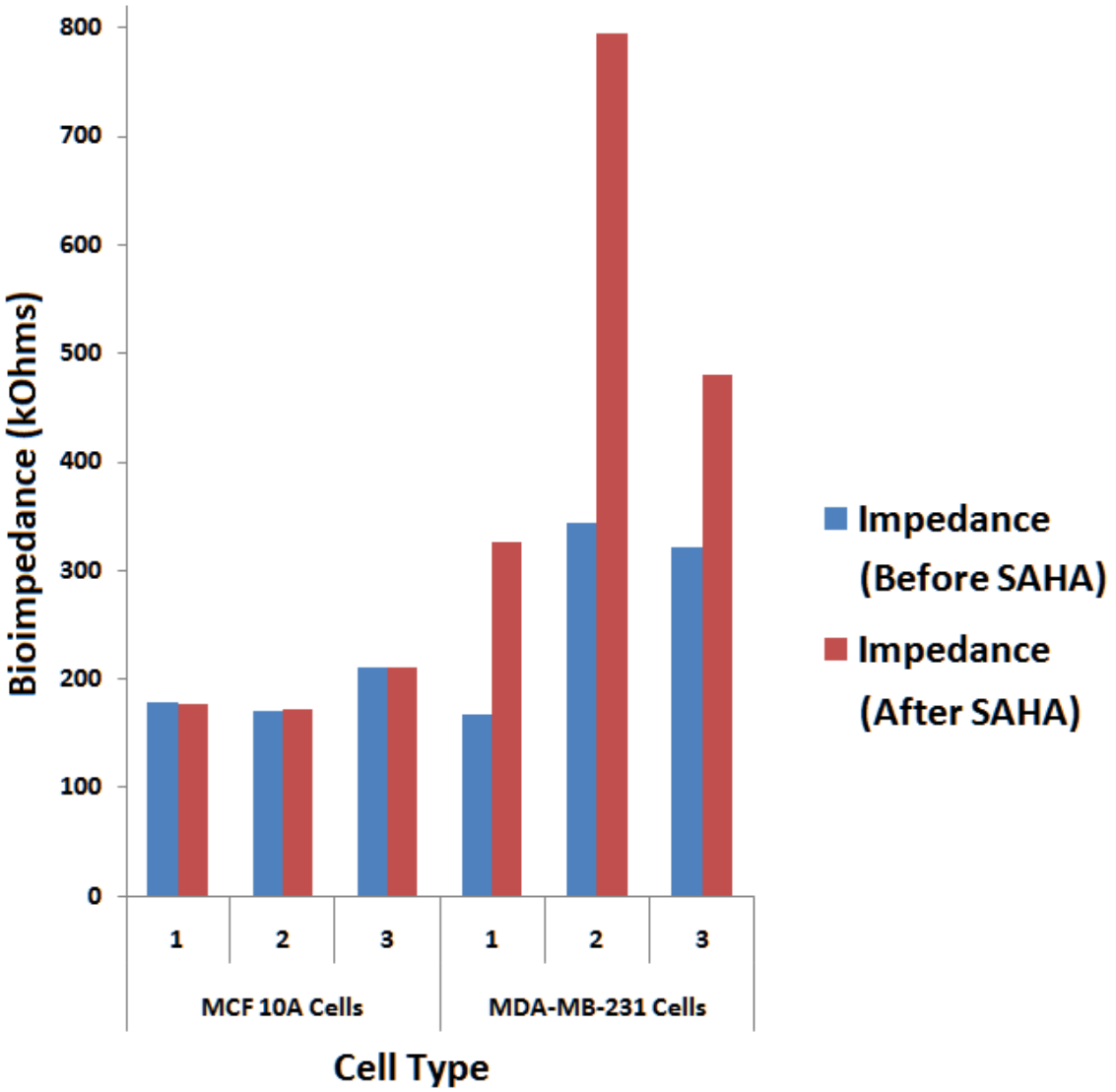

Figure 5.3. The bioimpedance changes due to SAHA (500 nM) on the cancer and normal cells types over three randomly selected electrodes from three experiments with four microelectrodes in each device.

The plot clearly shows no contribution to the increase in bioimpedance response from the MCF10A cells. Upon analysis, the percentage change in the average and median peak bioimpedance response of the two cell types was determined to be as following. There was a 50% average and 50% median increase, respectively, for MDA-MB-231 cells, which were larger than 4% average increase and 0.6% median decrease seen in MCF10A cells. The analysis was done over three experiments with the number of

functional electrodes analyzed for the three cell types being 9 for MDA-MB-231 and 12 for MCF10A cells respectively. The changes follow the trend seen in changes in mean cell area (Figure 3.4). It is proposed that the analysis of the median values provides a more useful end-point than the average values because it identifies how most cells in a population respond to SAHA. Although there are differences in the percentage changes in the average and median peak bioimpedance values for the MCF10A and HS68 cells, the median and average values for the MDA-MB-231 cells are consistent. Thus, it was concluded that the change in peak bioimpedance in response to 500nM SAHA is a reliable biomarker for MDA-MB-231 cell detection. Another important observation is that the peak bioimpedance for the control condition from all the electrodes shown for a particular cell type are not the same. This can be explained by the differences in cell coverage of the electrodes. In our experiments, a low plating density of cells was used and the electrodes were not covered with a confluent layer of cells when bioimpedance measurements were made. Thus, there were differences in the cell coverage of the electrodes based on the random process of cell adhesion on the electrodes.

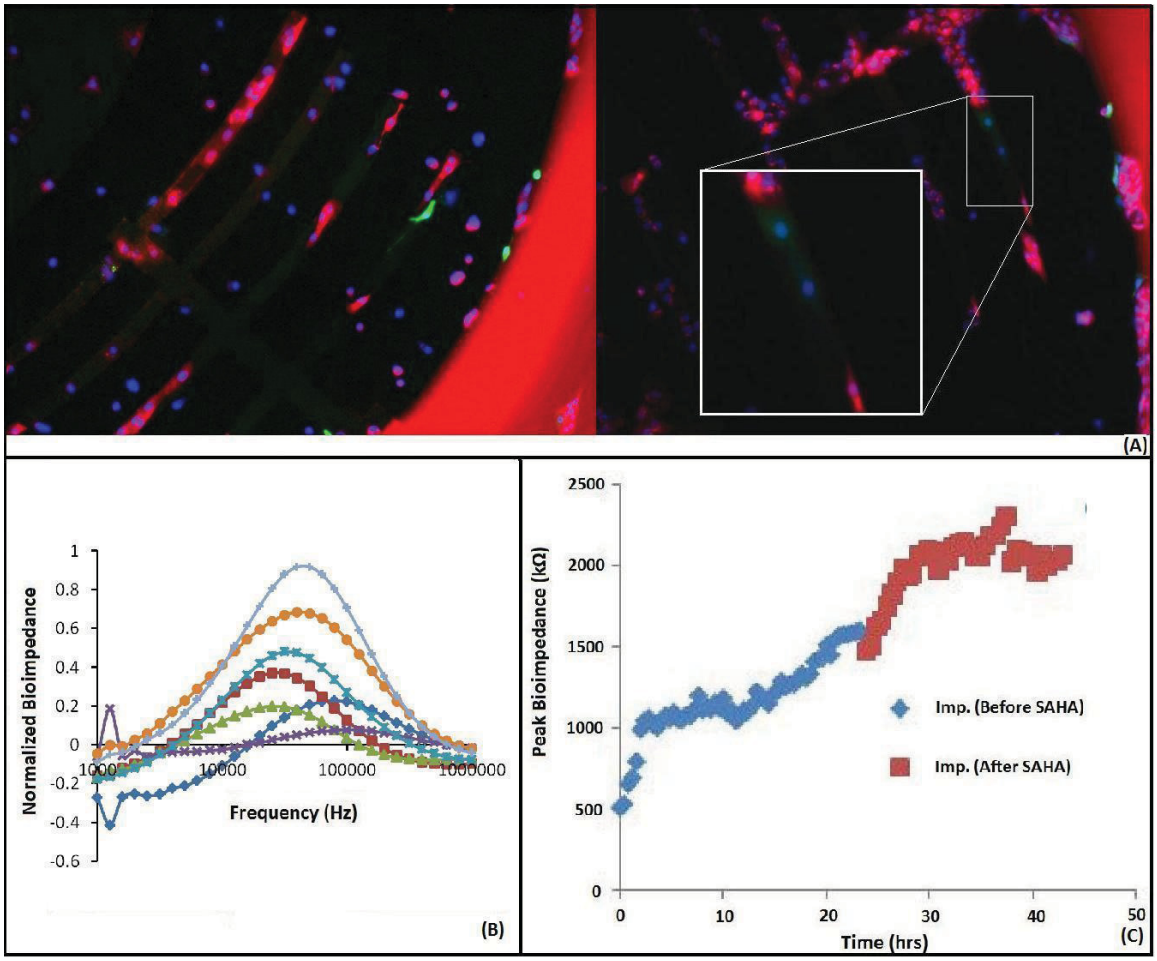

Figure 5.4. (A) Fluorescence images from a co-culture experiments (MCF10A cells – Red; MDA-MB-231 cells –green). (B) A typical plot of normalized impedance over the frequency range seen on all the electrodes from an experiment; each color represents a separate electrode. (C) The characteristic real-time changes in peak bioimpedance magnitude on a single electrode when SAHA was introduced.

Tests were then performed to check whether this bioimpedance response could identify the presence of a small number of cancer cells in a background of normal epithelial cells. Co-culture experiments were performed with different ratios of MDA-MB-231 and MCF10A cells, which were variations between 1:10 and 1:100 ratios of the two cells respectively. The cells of each type were counted on each electrode and correlated with the change in bioimpedance response elicited by SAHA. A 5% increase in the bioimpedance value measured at the peak was determined to be a reliable biomarker

for detection of cancer cells. Using this approach, we were able to detect the presence of a single cancer cell on an electrode when the ratio of cancer to normal cells on the electrode was as low as 0.01. Figure 5.4 shows fluorescence images from co-culture experiments and the typical impedance curves obtained from such experiments. These results were reported in the Transducer's 2011 conference in Beijing, China [51].

4.4 Discussion

Constrained spreading is confirmed in co-culture experiments as seen in Figure 5.4(A) on the right and has been highlighted for visibility. From experiments, the current measured sensitivity of each electrode in the sensor was found to be 0.01. This means that we were able to detect even a single cancer cell positioned on an electrode when around 100 or more other types of cells were present on the same electrode. A cancer cell present on any of the four electrodes in the sensor will be detected using this bioimpedance sensor. Thus, the sensitivity of the sensor is 25/10000 cancer/normal ratio. This value is further improved if we do not limit the number of normal cells on the three electrodes on which, no cancer cell is present. Hence the sensor, in theory, has a much higher actual sensitivity.

It is noteworthy that the cells from a sample culture randomly distribute themselves throughout the area of the sensor. The sensor also has a large counter electrode and any cancer cells that position themselves on it are not detected by the sensor. This implies that even though the sensor is highly sensitive, the number of cancer cells required in the sample might be much higher than the detection limit of the sensor as some cancer cells are lost in areas outside the sensing area of electrodes. Hence, there is a need to maximize electrode coverage within the area in which cells come in contact with the bioimpedance sensor. In our next generation of devices, we also plan to isolate the counter electrode area to ensure all cancer cells reside on the sensing area of the bioimpedance sensor.

In our experiments, we identified the concentration of SAHA (500 nM), which produced less than 5% change in the peak bioimpedance response from the MCF10A normal cells and used this concentration in co-culture experiments for cancer cell detection. There has been some research in the past concerning the effect of cell growth and attachment on the electrode modeled as changes in the cell coverage of the electrode and the gap between the cell and the substrate [52].We believe that other factors such as the cell-substrate gap are likely involved in the SAHA related bioimpedance increase in addition to the cytoskeletal alteration seen as a change in the mean cell area and length. Although drugs such as cytocholasin D, Nocodozole, Jasplakinolide and others alter the cytoskeleton of cells, the uniqueness of SAHA is that it is highly selective and thus makes it a promising approach for detection of sparsely present breast cancer cells.

6. Tri-cell Culture Model

HS 68 fibroblast cells were introduced in the cell culture and the experiments were repeated to characterize the sensor's detection limit and sensitivity for a tri-cell culture model with MDA-MB-231 metastatic breast cells, MCF 10A normal epithelial cells and HS 68 normal fibroblast cells. The following sections discuss the rationale behind including fibroblasts as the third cell type in our cell model, the experiments conducted, obtained results and a discussion

6.1. Rationale

Biopsy samples of human breast tissue are much more complex than the co-culture system in which single cancer cell detection was achieved. To demonstrate the capability of our system to handle complexity, we introduced HS68 fibroblast cells into our model system. It has been shown that tumor-associated fibroblast cells influence the growth and behavior of malignant breast epithelial cells [53] and it is proposed that their inclusion represents an improved cell culture model of a human biopsy sample.

6.2 Experiments

The experiments follow the same protocol described in chapter 4 for the MDA-MB-231 and MCF 10A cells. Please refer to section 4.2 for a detailed description. The bioimpedance sensor chip described in Chapter 5 and reduced 500 nM concentration of SAHA was used for all the tri-culture experiments. Here, we describe the handling of the HS 68 fibroblast cells. The HS68 cell line was also obtained from the American Type Culture Collections (ATCC). The HS68 cells were stained with CellTrace™ calcein red-orange dye from Invitrogen using methods recommended by the supplier in order to

enable fluorescence imaging of the cells at the end of each experiment. The cells were grown in T-75 cm^2 culture flasks in the incubator maintained at 37 ˚C and 5% CO2 using a cell culture medium consisted of RPMI and 10% FBS. In these experiments, the plating density of cells was set at 6000 cells/200µl; MDA-MB-231, MCF10A and HS68 cells were seeded at a ratio of 2:9:9. The resultant final cell density was 50-100 cells/electrode.

6.3 Results

Figure 6.1 shows the comparison of the changes observed in the peak bioimpedance of HS 68 fibroblast cells with the MCF 10A cells and the MDA-MB-231 cells in three randomly selected electrodes. The plot clearly shows no contribution to the increase in bioimpedance response from the MCF10A and HS68 cells. The analysis of the MDA-MB-231 and the MCF 10A cells has already been discussed in section 5.3. The HS68 cells showed an 11% average decrease and 5% median decrease in the peak bioimpedance value. The analysis was done over 8 functional electrodes in three experiments for HS68 cells. These changes also follow the trend seen in changes in mean cell area of HS 68 cells (Figure 4). Thus the inclusion of HS 68 fibroblast cells would not significantly affect the detection strategy developed.

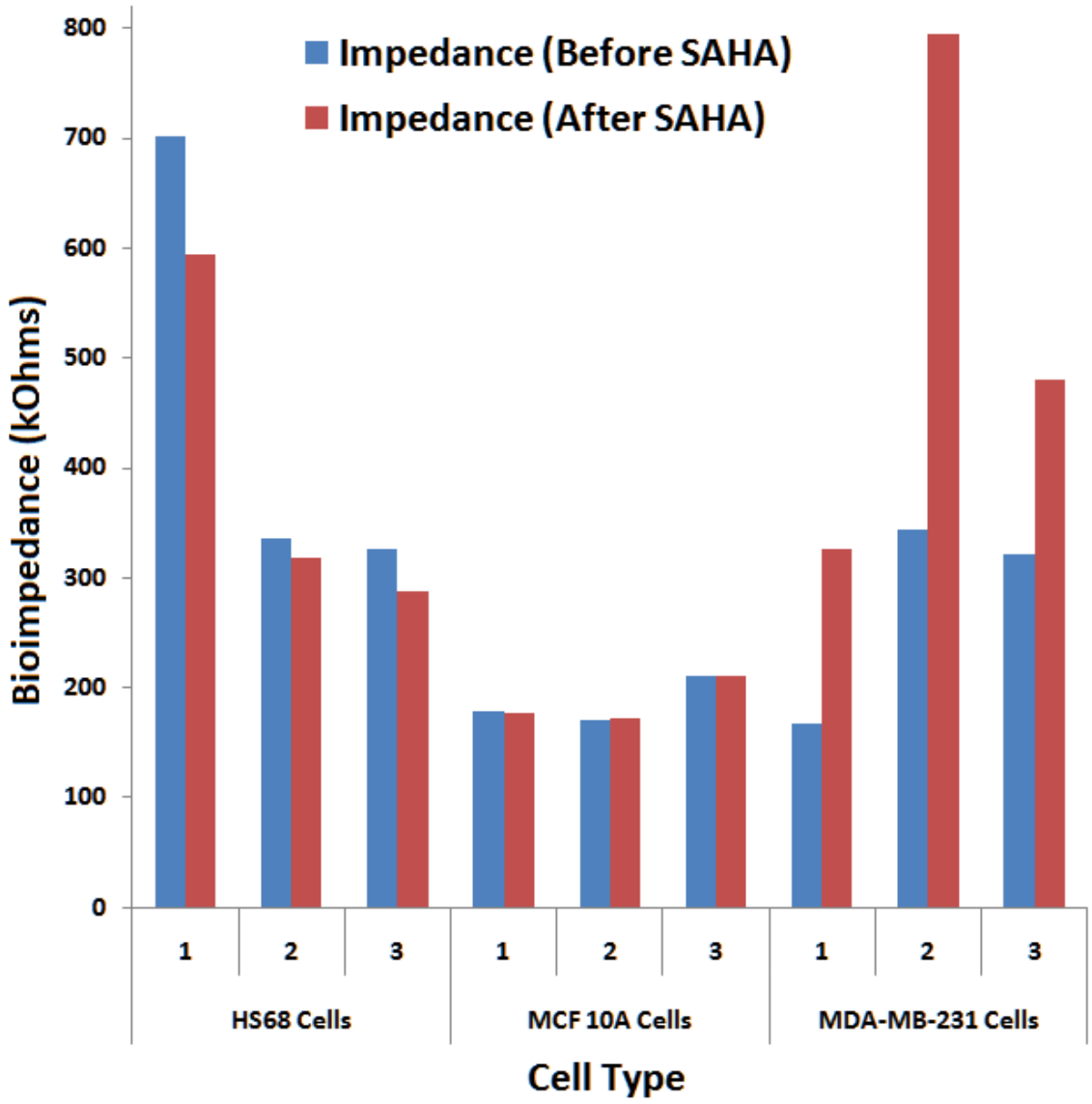

Figure 6.1. The changes in the peak bioimpedance seen due to 500 nM SAHA over three randomly selected electrodes for each of the three cell types.

Figure 6.2 shows cells in tri-culture on the electrode. All three cell types are distinguishable on the electrodes based on fluorescence and cell shape. Although MCF10A and HS68 cells are similar in color, their cuboidal and fibroblastoid morphologies, respectively, distinguish them. Cancer cells on each electrode were easily identified by their green fluorescence. The peak bioimpedance changes on electrodes

harboring cancer cells were compared with those observed on electrodes lacking cancer cells.

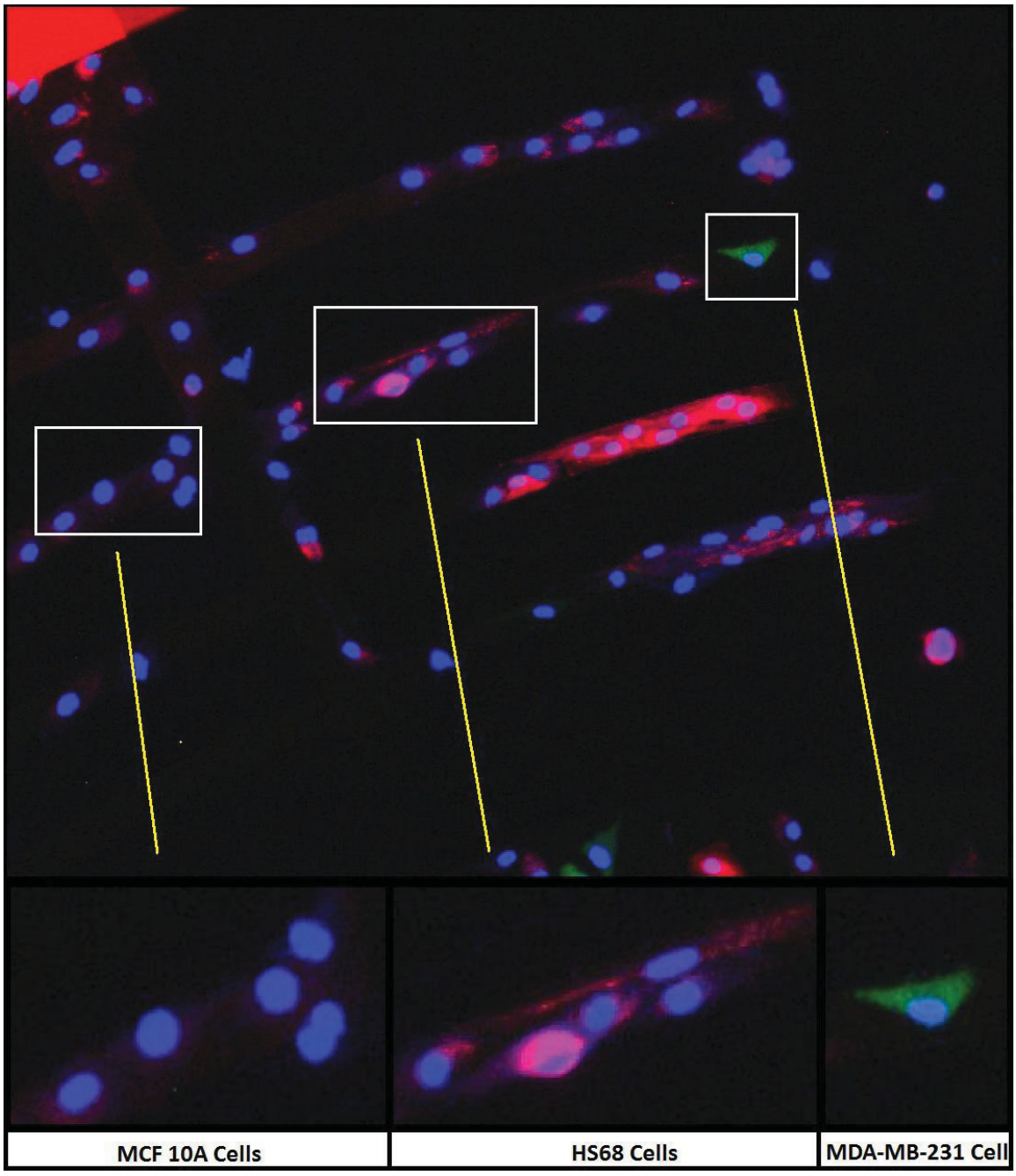

Figure 6.2. Fluorescence image highlighting the three cell types on an electrode in a tri-culture experiment.

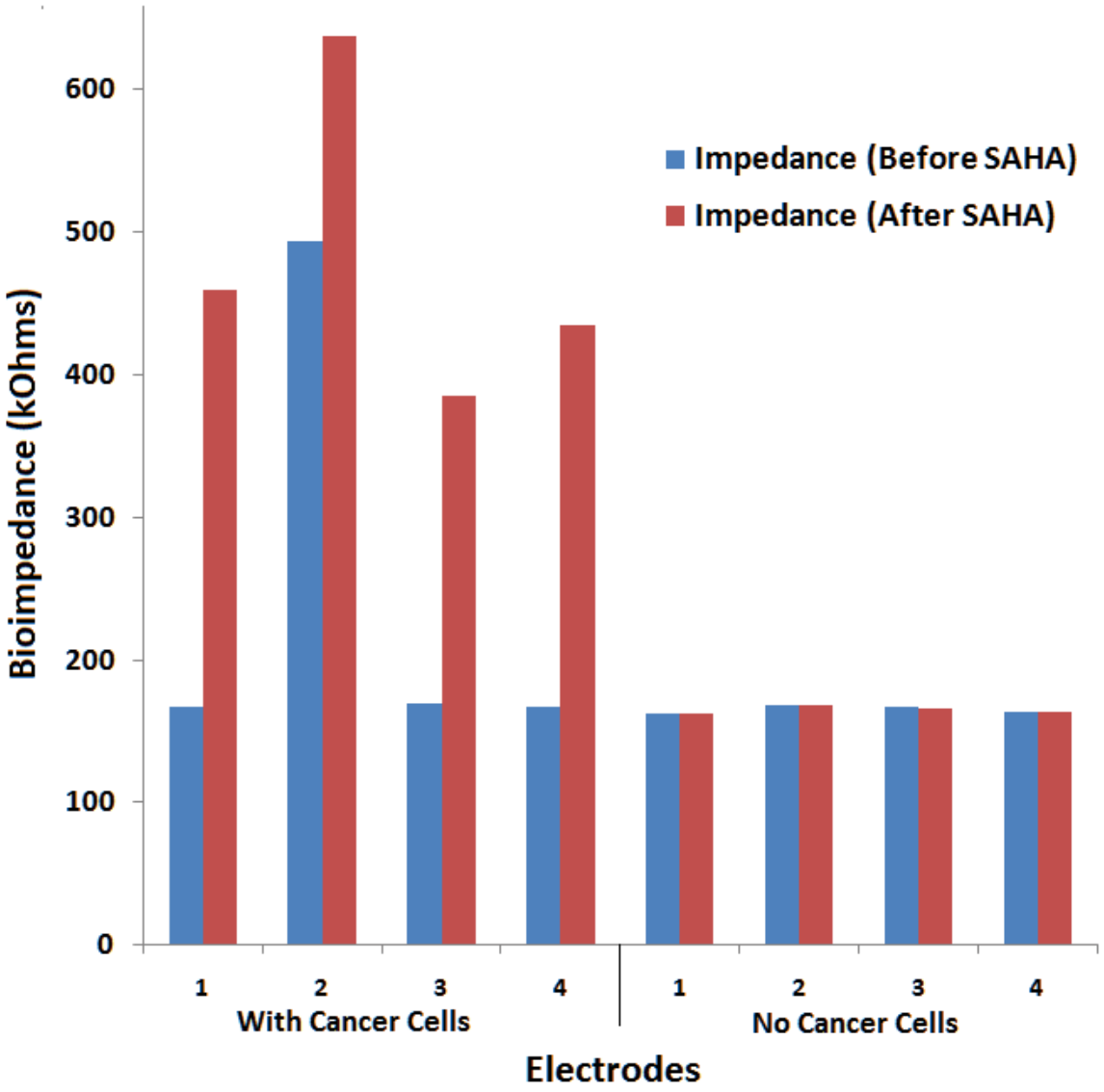

Figure 6.3. SAHA induced responses in the presence (electrodes 1-4) and absence (electrodes 5-8) of cancer cells on the peak bioimpedance in eight randomly selected electrodes.

Data collected from three experiments from eight randomly selected electrodes are shown in Figure 6.3. We report measurable increases in peak bioimpedance magnitude in the range of 29-174% when at least one cancer cell was present on the electrode in tri-culture. The average percentage increase in the peak bioimpedance was calculated to be 123% and the percentage increase in the median peak bioimpedance was 144% when cancer cells were present on the electrode. Interestingly, electrode 2 in

Figure 15 had a much larger initial response and a smaller increase in peak bioimpedance due to SAHA action on the cancer cell(s) present on it. Both of these observations could be attributed to a higher number of fibroblasts present on this electrode compared with that seen in other electrodes For example, refer to Figure 13 and compare with high initial bioimpedance response of fibroblast monocultures with the drop in peak bioimpedance after SAHA. These results were reported in the MicroTAS 2011 conference in Seattle, Washington [54].

6.4 Discussion

In our experiments, we identified the concentration of SAHA (500 nM), which produced less than 5% change in the peak bioimpedance response from the MCF10A normal cells and used this concentration in co-culture and tri-culture experiments for cancer cell detection. From monoculture experiments (Figure 6.1) we noted a decrease in peak bioimpedance for the HS68 cells when treated with SAHA (500 nM). This might result from continuous fluctuations in the bioimpedance response of the HS68 cells due to their detachment from the substrate during cell movement [55].

Although bioimpedance of cancer and normal cells has been studied by researchers in the past, the use of bioimpedance properties to detect cancer cells in co-culture and the bioimpedance analysis of a complex tri-cell culture system is presented here for the first time.

7. Conclusion

A bioimpedance sensor capable of detecting very few cancer cells in a background of normal epithelial and fibroblast cells was designed, fabricated and tested. Narrow branch electrodes were incorporated in our device to enhance its sensitivity to SAHA-induced cytoskeletal changes in cancer cells. SAHA, an FDA approved anti-cancer agent, was used to selectively alter the cytoarchitecture of cancer cells. This caused differential cell attachment and spreading of the cancer cells as compared to the normal and fibroblast cells. The resulting bioimpedance changes were used in cancer detection where the cancer to normal cell ratio on one electrode was as low as 1:100/electrode. Also, HS68 fibroblast cells were included in the cell model to better represent human samples and demonstrate the ability of the sensor to handle complex cell cultures. This is the first time cancer cell detection has been reported in a complex tri-culture on an ECIS-based biosensor chip. Future work is aimed at identifying the factors responsible for the bioimpedance changes associated with SAHA action on cancerous MDA-MB-231 cells, determining the detection limit for these devices, and exploring strategies to increase sensitivity in future generations of our bioimpedance sensor.

8. References

[1] A. C. Society, "Cancer: Facts and Figures 2010," ed. Atlanta , GA: American Cancer Society, 2010.

[2] H. Kim, J. Kwak, J. Choi, J. Bae, K. Shin, H. Lee, G. Kim, J. Jung, and J. Park, "Impact of US Surveillance on Detection of Clinically Occult Locoregional Recurrence after Mastectomy for Breast Cancer.," Annals of Surgical Oncology, April 27 2010.

[3] J. Wegener, C. R. Keese, and I. Giaever, "Electric cell-substrate impedance sensing (ECIS) as a noninvasive means to monitor the kinetics of cell spreading to artificial surfaces," Experimental Cell Research, vol. 259, pp. 158-166, Aug 2000.

[4] F. Asphahani, M. Thein, O. Veiseh, D. Edmondson, R. Kosai, M. Veiseh, J. Xu, and M. Q. Zhang, "Influence of cell adhesion and spreading on impedance characteristics of cell-based sensors," Biosensors & Bioelectronics, vol. 23, pp. 1307-1313, Mar 2008.

[5] P. Mitra, C. R. Keese, and I. Giaever, "Electric measurements can be used to monitor the attachment and spreading of cells in tissue-culture," Biotechniques, vol. 11, pp. 504-&, Oct 1991.

[6] L. Ghenim, H. Kaji, Y. Hoshino, T. Ishibashi, V. Haguet, X. Gidrol, and M. Nishizawa, "Monitoring impedance changes associated with motility and mitosis of a single cell," Lab on a Chip, vol. 10, pp. 2546-2550, 2010.

[7] I. Giaever and C. R. Keese, "Micromotion of mammalian-cells measured electrically," Proceedings of the National Academy of Sciences of the United States of America, vol. 90, pp. 1634-1634, Feb 1993.

[8] C. Xiao and J. H. T. Luong, "On-line monitoring of cell growth and cytotoxicity using electric cell-substrate impedance sensing (ECIS)," Biotechnology Progress, vol. 19, pp. 1000-1005, May-Jun 2003.

[9] F. Asphahani, K. Wang, M. Thein, O. Veiseh, S. Yung, J. A. Xu, and M. Q. Zhang, "Single-cell bioelectrical impedance platform for monitoring cellular response to drug treatment," Physical Biology, vol. 8, Feb 2011.

[10] A. M. Otto, M. Brischwein, E. Motrescu, and B. Wolf, "Analysis of drug action on tumor cell metabolism using electronic sensor chips," Archiv Der Pharmazie, vol. 337, pp. 682-686, Dec 2004.

[11] G. M. Dittami, H. E. Ayliffe, C. S. King, and R. D. Rabbitt, "A multilayer MEMS platform for single-cell electric impedance spectroscopy and electrochemical analysis," Journal of Microelectromechanical Systems, vol. 17, pp. 850-862, Aug 2008.

[12] C. V. Kurz, H. Buth, A. Sossalla, V. Vermeersch, V. Toncheva, P. Dubruel, E. Schacht, and H. Thielecke, "Chip-based impedance measurement on single cells for monitoring sub-toxic effects on cell membranes," Biosensors & Bioelectronics, vol. 26, pp. 3405-3412, Apr 2011.

[13] K. C. Lan and L. S. Jang, "Integration of single-cell trapping and impedance measurement utilizing microwell electrodes," Biosensors & Bioelectronics, vol. 26, pp. 2025-2031, Jan 2011.

[14] H. Morgan, T. Sun, D. Holmes, S. Gawad, and N. G. Green, "Single cell dielectric spectroscopy," Journal of Physics D-Applied Physics, vol. 40, pp. 61-70, Jan 2007.

[15] A. Han and A. B. Frazier, "Ion channel characterization using single cell impedance spectroscopy," Lab on a Chip, vol. 6, pp. 1412-1414, 2006.

[16] L. Vistejnova, J. Dvorakova, M. Hasova, T. Muthny, V. Velebny, K. Soucek, and L. Kubala, "The comparison of impedance-based method of cell proliferation monitoring with commonly used metabolic-based techniques," Neuroendocrinology Letters, vol. 30, pp. 121-127, 2009.

[17] Q. J. Liu, J. J. Yu, L. Xiao, J. C. O. Tang, Y. Zhang, P. Wang, and M. Yang, "Impedance studies of bio-behavior and chemosensitivity of cancer cells by micro-electrode arrays," Biosensors & Bioelectronics, vol. 24, pp. 1305-1310, Jan 2009.

[18] L. R. Arias, C. A. Perry, and L. J. Yang, "Real-time electrical impedance detection of cellular activities of oral cancer cells," Biosensors & Bioelectronics, vol. 25, pp. 2225-2231, Jun 2010.

[19] L. J. Yang, L. R. Arias, T. S. Lane, M. D. Yancey, and J. Mamouni, "Real-time electrical impedance-based measurement to distinguish oral cancer cells and non-cancer oral epithelial cells," Analytical and Bioanalytical Chemistry, vol. 399, pp. 1823-1833, Feb 2011.

[20] Y. Cho, H. S. Kim, A. B. Frazier, Z. G. Chen, D. M. Shin, and A. Han, "Whole-cell impedance analysis for highly and poorly metastatic cancer cells," Journal of Microelectromechanical Systems, vol. 18, pp. 808-817, Aug 2009.

[21] A. Han, L. Yang, and A. B. Frazier, "Quantification of the heterogeneity in breast cancer cell lines using whole-cell impedance spectroscopy," Clinical Cancer Research, vol. 13, pp. 139-143, Jan 2007.

[22] I. Giaever and C. R. Keese, "A morphological biosensor for mammalian-cells" Nature, vol. 366, pp. 591-592, Dec 1993.

[23] I. Giaever and C. R. Keese, "Monitoring fibroblast behavior in tissue-culture with an applied electric-field," Proceedings of the National Academy of Sciences of the United States of America-Biological Sciences, vol. 81, pp. 3761-3764, 1984 1984.

[24] R. Ehret, W. Baumann, M. Brischwein, A. Schwinde, K. Stegbauer, and B. Wolf, "Monitoring of cellular behaviour by impedance measurements on interdigitated electrode structures," Biosensors & Bioelectronics, vol. 12, pp. 29-41, 1997 1997.

[25] Y. Baumer, B. Scholz, S. Ivanov, and B. Schlosshauer, "Telomerase-based immortalization modifies the angiogenic/inflammatory responses of human coronary artery endothelial cells," Experimental Biology and Medicine, vol. 236, pp. 692-700, Jun 2011.

[26] S. David, C. C. Ghosh, P. Kuempers, N. Shushakova, P. Van Slyke, E. V. Khankin, S. A. Karumanchi, D. Dumont, and S. M. Parikh, "Effects of a synthetic PEG-ylated Tie-2 agonist peptide on endotoxemic lung injury and mortality," American Journal of Physiology-Lung Cellular and Molecular Physiology, vol. 300, pp. L851-L862, Jun 2011.

[27] C. M. Ebrahimi, T. R. Sheen, C. W. Renken, R. A. Gottlieb, and K. S. Doran, "Contribution of Lethal Toxin and Edema Toxin to the Pathogenesis of Anthrax Meningitis," Infection and Immunity, vol. 79, pp. 2510-2518, Jul 2011.

[28] J. Hong, K. Kandasamy, M. Marimuthu, C. S. Choi, and S. Kim, "Electrical cell-substrate impedance sensing as a non-invasive tool for cancer cell study," Analyst, vol. 136, pp. 237-245, 2011.

[29] W.-K. Lee, B. Torchalski, N. Kohistani, and F. Thevenod, "ABCB1 protects kidney proximal tubule cells against cadmium-induced apoptosis: Roles of cadmium and ceramide transport," Toxicological Sciences, vol. 121, pp. 343-356, Jun 2011.

[30] S. Rangasamy, R. Srinivasan, J. Maestas, P. G. McGuire, and A. Das, "A potential role for angiopoietin 2 in the regulation of the blood-retinal barrier in diabetic retinopathy," Investigative Ophthalmology & Visual Science, vol. 52, pp. 3784-3791, May 2011.

[31] G. Stokman, Y. Qin, H.-G. Genieser, F. Schwede, E. de Heer, J. L. Bos, I. M. Bajema, B. van de Water, and L. S. Price, "Epac-rap signaling reduces cellular stress and ischemia-induced kidney failure," Journal of the American Society of Nephrology, vol. 22, pp. 859-872, May 2011.

[32] G. E. White, E. McNeill, I. Christou, K. M. Channon, and D. R. Greaves, "Site-directed mutagenesis of the CC chemokine binding protein 35K-Fc reveals residues essential for activity and mutations that increase the potency of CC chemokine blockade," Molecular Pharmacology, vol. 80, pp. 328-336, Aug 2011.

[33] X. Zhang, F. Tan, V. Brovkovych, Y. Zhang, and R. A. Skidgel, "Cross-talk between carboxypeptidase M and the kinin B1 receptor mediates a new mode of G protein-coupled receptor signaling," Journal of Biological Chemistry, vol. 286, pp. 18547-18561, May 27 2011.

[34] S. Matsumoto, Y. Arakawa, M. Ohishi, H. Yanaihara, T. Iwanaga, and N. Kurokawa, "Suppressive action of pituitary adenylate cyclase activating polypeptide (PACAP) on proliferation of immature mouse Leydig cell line TM3 cells," Biomedical Research-Tokyo, vol. 29, pp. 321-330, Dec 2008.

[35] Y. Ke, D. Wu, F. Princen, T. Nguyen, Y. Pang, J. Lesperance, W. J. Muller, R. G. Oshima, and G. S. Feng, "Role of Gab2 in mammary tumorigenesis and metastasis," Oncogene, vol. 26, pp. 4951-4960, Jul 2007.

[36] Z. Xie, E. J. Vallender, N. Yu, S. L. Kirstein, H. Yang, M. E. Bahn, S. V. Westmoreland, and G. M. Miller, "Cloning, expression, and functional analysis of rhesus monkey trace amine-associated receptor 6: Evidence for lack of monoaminergic association," Journal of Neuroscience Research, vol. 86, pp. 3435-3446, Nov 15 2008.

[37] Y. A. Abassi, J. A. Jackson, J. Zhu, J. O'Connell, X. B. Wang, and X. Xu, "Label-free, real-time monitoring of IgE-mediated mast cell activation on microelectronic cell sensor arrays," Journal of Immunological Methods, vol. 292, pp. 195-205, Sep 2004.

[38] J. M. Atienza, N. Yu, X. Wang, X. Xu, and Y. Abassi, "Label-free and real-time cell-based kinase assay for screening selective and potent receptor tyrosine kinase inhibitors using microelectronic sensor array," Journal of Biomolecular Screening, vol. 11, pp. 634-643, Sep 2006.

[39] J. Zhang, H. N. Ren, P. Yuan, W. H. Lang, L. Zhang, and L. Mao, "Down-regulation of hepatoma-derived growth factor inhibits anchorage-independent growth and invasion of non-small cell lung cancer cells," Cancer Research, vol. 66, pp. 18-23, Jan 1 2006.

[40] J. Wang, M. Bhutani, A. K. Pathak, W. Lang, H. Ren, J. Jelinek, R. He, L. Shen, J.-P. Issa, and L. Mao, "Delta DNMT3B variants regulate DNA methylation in a promoter-specific manner," Cancer Research, vol. 67, pp. 10647-10652, Nov 15 2007.

[41] N. M. Hawsawi, H. Ghebeh, S.-F. Hendrayani, A. Tulbah, M. Al-Eid, T. Al-Tweigeri, D. Ajarim, A. Alaiya, S. Dermime, and A. Aboussekhra, "Breast carcinoma - Associated fibroblasts and their counterparts display neoplastic-specific changes," Cancer Research, vol. 68, pp. 2717-2725, Apr 15 2008.

[42] P. F. Davies, A. Robotewskyj, and M. L. Griem, "Endothelial-cell adhesion in real-time - Measurements invitro by tandem scanning confocal image-analysis," Journal of Clinical Investigation, vol. 91, pp. 2640-2652, Jun 1993.

[43] A. A. Lane and B. A. Chabner, "Histone deacetylase inhibitors in cancer therapy," Journal of Clinical Oncology, vol. 27, pp. 5459-5468, Nov 10 2009.

[44] P. A. Marks and R. Breslow, "Dimethyl sulfoxide to vorinostat: Development of this histone deacetylase inhibitor as an anticancer drug," Nature Biotechnology, vol. 25, pp. 84-90, Jan 2007.

[45] J. Tan, S. Cang, Y. Ma, R. L. Petrillo, and D. Liu, "Novel histone deacetylase inhibitors in clinical trials as anti-cancer agents," Journal of Hematology & Oncology, vol. 3, Feb 4 2010.

[46] J. Gardner, C. Introcaso, S. Nasta, E. Kim, C. Vittorio, and A. Rook, "A novel regimen of vorinostat with interferon gamma for refractory Sézary syndrome," Journal of the American Academy of Dermatology, vol. Volume 61, pp. 112-116, 2009.

[47] E. Galanis, K. A. Jaeckle, M. J. Maurer, J. M. Reid, M. M. Ames, J. S. Hardwick, J. F. Reilly, A. Loboda, M. Nebozhyn, V. R. Fantin, V. M. Richon, B. Scheithauer, C. Giannini, P. J. Flynn, D. F. Moore, Jr., J. Zwiebel, and J. C. Buckner, "Phase II trial of vorinostat in recurrent glioblastoma multiforme: A north central cancer treatment group study (vol 27, pg 2052, 2009)," Journal of Clinical Oncology, vol. 27, pp. 3262-3262, Jul 1 2009.

[48] G. Egger, G. N. Liang, A. Aparicio, and P. A. Jones, "Epigenetics in human disease and prospects for epigenetic therapy," Nature, vol. 429, pp. 457-463, May 2004.

[49] J. S. Strobl, M. Nikkhah, and M. Agah, "Actions of the anti-cancer drug suberoylanilide hydroxamic acid (SAHA) on human breast cancer cytoarchitecture in silicon microstructures," Biomaterials, vol. 31, pp. 7043-7050, Sep 2010.

[50] S. Narayanan, M. Nikkhah, J. S. Strobl, and M. Agah, "Analysis of the passivation layer by testing and modeling a cell impedance micro-sensor," Sensors and Actuators a-Physical, vol. 159, pp. 241-247, May 2010.

[51] V. Srinivasaraghavan, J. Strobl, and M. Agah, "Chemical induced impedance spectroscopy for single cancer cell detection," presented at the Transducers', Beijing, China, 2011.

[52] X. Q. Huang, D. Nguyen, D. W. Greve, and M. M. Domach, "Simulation of microelectrode impedance changes due to cell growth," Ieee Sensors Journal, vol. 4, pp. 576-583, Oct 2004.

[53] A. Sadlonova, Z. Novak, M. R. Johnson, D. B. Bowe, S. R. Gault, G. P. Page, J. V. Thottassery, D. R. Welch, and A. R. Frost, "Breast fibroblasts modulate epithelial cell proliferation in three-dimensional in vitro co-culture," Breast Cancer Research, vol. 7, pp. R46-R59, 2005.

[54] V. Srinivasaraghavan, J. Strobl, and M. Agah, "Detection of breast cancer cells in tri-culture using impedance spectroscopy," presented at the 15th International Conference on Miniaturized Systems for Chemistry and Life Sciences, Seattle, WA, 2011.

[55] W. T. Chen, "Mechanism of retraction of the trailing edge during fibroblast movement," Journal of Cell Biology, vol. 90, pp. 187-200, 1981.